Atmos. Chem. Phys. Discuss., 12, 21815–21865, 2012
www.atmos-chem-phys-discuss.net/12/21815/2012/
doi:10.5194/acpd-12-21815-2012

Atmospheric Chemistry and Physics Discussions

Modeling meteorological and chemical effects of secondary organic aerosol during an EUCAARI campaign

E. Athanasopoulou[1], H. Vogel[1], B. Vogel[1], A. Tsimpidi[2], S. N. Pandis[3], C. Knote[4], and C. Fountoukis[3]

[1]Institute for Meteorology and Climate Research, Karlsruhe Institute of Technology, Karlsruhe, Germany
[2]School of Earth and Atmospheric Sciences, Georgia Institute of Technology, Atlanta, GA, USA
[3]Institute of Chemical Engineering and High Temperature Chemical Processes, Foundation for Research and Technology Hellas (FORTH), Patras, Greece
[4]Laboratory for Air Pollution/Env. Technology, Empa Materials and Science, 8600 Duebendorf, Switzerland

Received: 26 July 2012 – Accepted: 15 August 2012 – Published: 23 August 2012

Correspondence to: E. Athanasopoulou (eleni.athanasopoulou@kit.edu);
B. Vogel (bernhard.vogel@kit.edu)

Published by Copernicus Publications on behalf of the European Geosciences Union.

Abstract

A Volatility Basis Set (VBS) approach for Secondary Organic Aerosol (SOA) formation is incorporated in the online coupled atmospheric model system COSMO-ART and applied over Europe during the EUCAARI May 2008 campaign. Organic Aerosol (OA) performance is improved when compared to the default SOA module of COSMO-ART (SORGAM) against high time resolution Aerosol Mass Spectrometer (AMS) ground measurements. This allows the investigation of SOA impact upon the radiative budget. The mean direct surface radiative cooling averaged over Europe is $-1.2\,W\,m^{-2}$ and contributes by about 20 % to the total aerosol effect. Nevertheless, responses are not spatially correlated with the forcing, due to the nonlinear interactions among changes in particle chemical composition, water content, size distribution and cloud cover. These interactions initiated by the effect of SOA on radiation result even in a positive forcing over a limited surface and mostly where the net effect of interactions on the cloud cover is negative. Further model experiments showed that nitrogen oxides availability slightly affects SOA production, but the aging rate constant within the VBS approximation and the boundary concentrations assumed in the model should be carefully selected. SOA aging is found to reduce hourly nitrate levels up to 30 %, while the condensation upon pre-existing, SOA-rich particles result in a monthly average increase of 5 % in sulfate and ammonium formation in the accumulation mode.

1 Introduction

Organic Aerosol (OA) is a significant, if not the most important, fraction of submicron particles (PM1) on a global scale (Zhang et al., 2007). Organic matter can exist in the particle phase from the moment of its emission as Primary Organic Aerosol (POA), which is created mainly by combustion, and as Secondary Organic Aerosol (SOA): Volatile Organic Compounds (VOCs) and POA are oxidized in the atmosphere and complex chemical mixtures of a large number of SOA are formed (Robinson

ACPD
12, 21815–21865, 2012

et al., 2007). OA measurements distinguish hydrogenated (HOA) and Oxidized Organic Aerosol (OOA), and it is found that there is a strong correlation of HOA to POA, and of OOA to SOA. Jimenez et al. (2009) argue that the atmospheric OOA evolves through a dynamic aging process of continual repartitioning between the particle and gas phases (chemical aging), which leads to a more oxidized, less volatile and more hygroscopic aerosol. The deconvolution of OA measurements into HOA and OOA constituents showed the importance of the latter, which reaches more than 80 % and 95 % of the total OA in urban downwind, and remote sites, respectively (Zhang et al., 2007; Morgan et al., 2012b).

Recent studies have shown that OA concentrations are often underestimated, when semi-volatile compounds are not included in global and regional chemical transport models (Volkamer et al., 2006; Dzepina et al., 2009; O'Donnell et al., 2011). An efficient way to describe the chemical evolution of thousands of organic compounds in models is their treatment as lumped species that span a range of effective saturation concentrations (Donahue et al., 2006). Recent model applications using different Volatility Basis Set (VBS) approaches confirm model's improved ability in predicting OA mass (Murphy and Pandis, 2009; Tsimpidi et al., 2010, 2011; Shrivastava et al., 2011; Farina et al., 2010; Murphy et al., 2011; Fountoukis et al., 2011; Bergström et al., 2012).

Oxidised organic aerosol has significant implications for the radiative budget in a wide range of continental environments (Kanakidou et al., 2005; Tsigaridis et al., 2005; Chen et al., 2009). When mixed with inorganic components and soot, it increases aerosol scattering and contributes to its negative direct radiative forcing (Ming et al., 2005; Forster et al., 2007; Myhre et al., 2009; O' Donnell et al., 2011). Aerosol extinction increases due to organic matter are mostly driven by the large amount of associated water, as well as the enhanced mass due to condensation, which results in an increase in the mean particle diameter (Morgan et al., 2010a). The indirect impact of condensing organics involves the efficient growth of freshly nucleated particles to Cloud Condensation Nuclei (CCN) sizes in pristine areas and CCN decreases in polluted areas (Pierce et al., 2012; O'Donnell et al., 2011).

ACPD
12, 21815–21865, 2012

Under cloudy conditions, the pure radiative effects of aerosol are superposed by semi-direct processes (Vogel et al., 2009). For example, dust aerosols absorb solar and infrared radiation, heat and change the stability of the atmosphere, thereby influencing cloud formation, and in turn affect aerosol radiative forcing (Han et al., 2012). The nonlinearity involved in the feedbacks among such processes has an uncertain climate impact (Johnson et al., 2004; Penner et al., 2003). Under clear-sky conditions particles are exposed to incoming radiation and their cooling effect is intensified. On the contrary, radiative forcing in a standard (total-sky) situation is weakened by extinction over the areas covered by clouds (Ming et al., 2005; Han et al., 2012). In such cases, cloud optical depth is found higher than aerosol optical depth, it dominates radiation changes and is responsible for almost uncorrelated fields of aerosol concentration fields and radiation (Vogel et al., 2009).

The challenge of accurately modeling semi-volatile organic compounds is likely to be a significant deficiency in attempts to constrain the direct radiative forcing by aerosols. This is due to our limited understanding of the principal SOA precursor gases including the relative contribution of biogenic and anthropogenic VOCs, the magnitude of their emissions and the dominant SOA formation mechanisms (Carslaw et al., 2010). The uncertainty in the radiative impact of aerosol imposed by this lack of knowledge is liable to be greatest in areas where OA is a major component of the aerosol burden or during major pollution episodes (Morgan et al., 2010a).

In the framework of this study, organic aerosol estimations are performed by the regional atmospheric model COSMO-ART (Vogel et al., 2009). Gas-phase chemistry and aerosol processes are altered to include a modified VBS scheme in an attempt to overcome previous OA underestimations. The European Aerosol Cloud Climate and Air Quality Interactions (EUCAARI) measurements of organic aerosol during May 2008 are used to evaluate the new model version. Unlike all previous modelling studies over Europe (e.g. Andersson-Skold and Simpson, 2001; Simpson et al., 2007; Bessagnet et al., 2008; Fountoukis et al., 2011; Bergström et al., 2012), the interactive coupling of meteorology and chemistry within COSMO-ART enables an assessment of the direct

ACPD
12, 21815–21865, 2012

radiative forcing of organic aerosol predicted by the VBS scheme. In parallel, simulations of selected scenarios are made to test the response of OA predictions on several parameters of this VBS version. Inter-comparisons with a conventional SOA scheme and with a VBS-including air quality model evaluate the performance of different modelling approaches. Further model experiments aim at estimating the relative contribution of biogenic and anthropogenic sources to the formation of organic matter in the atmosphere and at examining whether the chemical aging of SOA affects secondary inorganic aerosol formation.

2 Model description

2.1 COSMO-ART

This study uses the regional atmospheric model COSMO-ART (Vogel et al., 2009) (ART stands for Aerosols and Reactive Trace gases), online-coupled to the COSMO regional numerical weather prediction and climate model (Baldauf et al., 2011). The online coupling is realized in a consistent way using the same spatial and temporal resolution for all scalars (temperature, radiative fluxes, gas and aerosol concentrations etc.). For processes affecting all scalars, as for example advection, the same numerical schemes are applied. Detailed model description can be found in the aforementioned and other publications (Stanelle et al., 2010; Bangert et al., 2012; Knote et al., 2011).

The gaseous chemistry in COSMO-ART is simulated by a modified version of the Regional Acid Deposition Model, Version 2 (RADM2) mechanism (Stockwell et al., 1990), which is extended to describe secondary organic aerosol formation (Schell et al., 2001) and hydroxyl recycling due to isoprene chemistry (Geiger et al., 2003). Aerosols are represented by the modal aerosol module MADE (Ackermann et al., 1998), improved by explicit treatment of soot aging through condensation of inorganic (Riemer et al., 2003) and organic substances. The five modes that represent the aerosol population contain: pure soot, secondary mixtures of sulfates, nitrates, ammonium, organ-

ACPD
12, 21815–21865, 2012

ics and water (nucleation and accumulation mode), and the internal mixtures of all these species in both modes. The transfer of aerosol species among these mixtures is achieved through condensation and coagulation. A separate coarse mode contains additional primary anthropogenic emitted particles. Meteorologically-affected emissions are also online-coupled to the model system. Sea-salt and desert dust emission algorithms are described in Vogel et al. (2006, 2009). The biogenic VOC emissions are calculated as functions of the land use type based on the Global Land Cover 2000 dataset (Bartholome and Belward, 2005) and the modeled temperatures and radiative fluxes (Vogel et al., 1995). Sedimentation, advection, washout and turbulent diffusion can modify the aerosol distributions.

The partitioning of the inorganic aerosol components between the gas and particulate phases is simulated by the ISORROPIA II module (Fountoukis and Nenes, 2007). Since organic aerosol is the main interest of this study, the description of the secondary organic aerosol chemistry and of the organic mass transfer between phases, is separately provided in the next section.

COSMO-ART is fully online-coupled, and allows for feedbacks of aerosols on temperature, radiation and CCN. Analytical description of the modules incorporated for this purpose exists in Vogel et al. (2009) and Bangert et al. (2011). The radiation scheme used within the model to calculate the vertical profiles of the short- and longwave radiative fluxes is GRAALS (Ritter and Geleyn, 1992). Aerosol forcing on the radiative budget involves several nonlinear feedback mechanisms. Radiative fluxes are modified by the aerosol water content mass and particle size distributions. This results in changes in the atmospheric temperature, and subsequently in humidity, cloud distributions, precipitation, wash out and aerosol mass concentrations. The chemical composition and mass of particles is also affected by the photolysis rates, which are a function of radiative fluxes.

The spectral range covered by GRAALS is 0.25 to 104.5 µm, divided in eight bands. The calculation of radiative fluxes depends on three aerosol optical properties: extinction coefficients, single scattering albedo and asymmetry parameters for each of the

ACPD
12, 21815–21865, 2012

five modes mentioned above, in each of the eight bands. These data have been calculated by applying the Mie theory through the code by Bohren and Huffman (1983). The input data used are the initial modal geometric mean diameters and the complex refractive indices of each chemical constituent in each mode. The initialization and calculation of the size distribution of each mode, as well as refractive indices for ammonium sulfate, nitrate and water are given in Riemer et al. (2003). Refractive indices for soot and organics are provided in Baeumer et al. (2007). Specifically for organics, the complex refractive index varies from $1.54 + 0.03i$ at a wavelength of 250 nm, to $1.50 + 1.1\ 10^{-5}i$ (at 1.4 µm) and to $1.50 + 0.02i$ (at 4 µm). These data are similar to calculated values for SOA coating on soot particles (Schnaiter et al., 2005). In the long wave range, the refractive index is set to $2.0 + 0.1i$. The Mie code was applied offline because of the computational cost for calculations at each grid point and time step. The parameters derived from this procedure and used by GRAALS, are given in Vogel et al. (2009).

2.2 Secondary organic aerosol modules

In the version of COSMO-ART applied for the current study, there is the option of choosing between two different SOA modules: the SORGAM which is the default SOA module of COSMO-ART, analytically described in Schell et al. (2001) and has been used in several applications (Grell et al., 2005; Stern et al., 2008; Elleman and Covert, 2009; Zhao et al., 2011; Chuang et al., 2011; Herwehe et al., 2011) and the VBS, which is the newly applied SOA module in COSMO-ART, based on the framework proposed by Donahue et al. (2006) and already applied in other models (Robinson et al., 2007; Lane et al., 2008; Murphy and Pandis, 2009; Tsimpidi et al., 2010, 2011; Shrivastava et al., 2011).

The SORGAM module incorporates eight SOA precursors: aromatics, higher alkanes, higher alkenes (six anthropogenic species) and terpenes (two biogenic species). These species are oxidized by the hydroxyl radical (OH), ozone (O_3) and nitrate radical (NO_3) through seventeen reactions (Table 1), forming eight condensable products

ACPD
12, 21815–21865, 2012

(four of anthropogenic and four of biogenic origin), which then partition between the gas and aerosol phases. The saturation concentration depends on any pre-existing internal mixture of aerosol compounds and on the saturation vapor pressure of each compound at ambient temperature conditions. Each added SOA species can exist in the nucleation and accumulation pure and mixed aerosol modes, thus the total number of the SOA species in COSMO-ART when coupled with SORGAM is 32.

The VBS approach applied in COSMO-ART uses the same precursors assumed by SORGAM, plus isoprene due to recent findings on its role regarding SOA formation (Liao et al., 2007; Karl et al., 2009; Robinson et al., 2011). The oxidation reactions of these VOCs (Table 1) produce four condensable species, grouped by their effective saturation concentration of 1, 10, 100 and 1000 $\mu g\,m^{-3}$ at 298 K. The four-product set was suggested by Lane et al. (2008) as satisfactory for the separate representation of the biogenic and anthropogenic organic matter in the boundary layer for urban and regional pollution modeling. This number of products was regarded reasonable and is found realistic (Sect. 4.2) and computationally efficient, because the total number of SOA species is halved when COSMO-ART is coupled with VBS, compared to using SORGAM. However, the number of volatility bins and reactions used by the VBS theory may vary from two (Shrivastava et al., 2011) to nine (Robinson et al., 2007) depending on the desired chemical resolution.

These four SOA bins represent mixtures of both anthropogenic and biogenic species, unlike all aforementioned studies. This approximation is better suited for computationally expensive models such as COSMO-ART running coupled cloud-aerosol-meteorology. Nevertheless, it does not deprive the model's capability from identifying the strength of each type of source. Results towards this direction are presented in Sect. 4.4.5. The yields used for the production of the four SOA species by the oxidation of their VOC precursors were measured during recent smog chamber experiments and are given in the Table 2.

The gas-to-particle mass transfer method used is kept as in SORGAM applications, but using the fixed saturation concentrations for the surrogates, localized in respect to

ACPD
12, 21815–21865, 2012

ambient air temperature and to the vaporization enthalpy of $\Delta H_{vap} = 75\,kJmol^{-1}$. The chemical aging of mixed SOA species is represented by their oxidation reactions with OH, using an aging rate constant of $k = 2.5 \times 10^{-12}\,cm^3\,mol^{-1}s^{-1}$ (Murphy et al., 2011). During each time step SOA species become less volatile by one order of magnitude. This mass, modestly increased to account for the added oxygen (7.5 % per reaction), is added to the respective SOA species preexisting from previous time step.

At this point it should be noted that a similar approach for SOA aging can be applied for POA, as already proposed in the literature (Shrivastava et al., 2008; Tsimpidi et al., 2010, 2011). Nevertheless, measurements indicate that HOA oxidation is not an important source of OOA, and that the latter reflects mainly SOA (Zhang et al., 2007). Thus, POA are treated as non-volatile by this VBS approach.

3 Application

Modeling simulations are performed over Europe for May 2008, when continuous and high temporal resolution measurements from various sites are available. The simulation area (Fig. 1) is covered by a grid (332 × 328 cells) with a horizontal resolution of 14 km. Vertically, there are 40 layers extending to 20 km, with the first layer being approximately 20 m thick. The meteorological initial and boundary conditions are obtained by the GME global model (Majewski et al., 2002) with an update frequency of 6 h. Boundary data for gas-phase species (carbon monoxide: CO, nitric acid: HNO_3, ammonia: NH_3, nitrogen oxides: NO_x = nitric oxide: NO + nitrogen dioxide: NO_2, NO_3, sulfur dioxide: SO_2, ozone: O_3, Non-Methane Volatile Organic Compounds: NMVOC), are provided through simulations of the MOZART global model (Emmons et al., 2010) with an update frequency of 6 h. For aerosol mass, constant boundary concentrations are used for the secondary species in the aged modes: $1\,\mu g\,m^{-3}$ for sulfates, $0.1\,\mu g\,m^{-3}$ for nitrates, $0.37\,\mu g\,m^{-3}$ for ammonium and $1\,\mu g\,m^{-3}$ for SOA in the surface layer (number concentrations are calculated consistently). The volatility concentration of the latter is assumed as 1 (half of the mass) and $10\,\mu g\,m^{-3}$. All values are vertically decreased

ACPD
12, 21815–21865, 2012

following the air density profile. Anthropogenic emissions used (CO, NH_3, NO_2, NO, sulfuric acid, SO_2, NMVOC, elemental and organic carbon, primary sulfate) are based on the TNO/MACC inventory (Kuenen et al., 2011; Denier van der Gon et al., 2010). Hourly emission values for two representative diurnal cycles (weekday and weekend) are derived from TNO/MACC values of 2007, scaled to 2008 employing per-species country totals as reported to EMEP (http://www.emep.int). A detailed description of its treatment for COSMO-ART can be found in Knote et al. (2011). The one month period is covered by 5-day successive simulations, in order to reinitialize meteorological fields with the GME analysis data. The first 2 days of May are used as a spin-up, to dampen the effect of initial conditions for gases and aerosol.

3.1 Model scenarios

Enhanced pollution conditions are exacerbated by the partitioning of semi-volatile precursors to the particle phase, causing a large increase in the aerosol direct radiative forcing. Thus, the period identified by this study is an ideal case to test regional and global climate model representations of the European area (Morgan et al., 2010a). In order to quantify the direct radiative forcing initiated by the VBS organic aerosol representation in COSMO-ART, an additional one-month simulation was performed with secondary organic aerosol chemistry switched off (scenario 1). Deviations from the baseline predictions for several atmospheric parameters (cloud cover, radiation, air temperature etc.) reflect changes originating from SOA formation over Europe by the VBS scheme (Sect. 4.3).

Apart from the baseline one-month application and scenario 1 performed as already described, six additional simulations were carried out, using shorter periods when possible. A summary of all simulations can be found in Table 3.

Since OA is supposed to reach a stable oxidation state in one to three days of transport (Hildebrandt et al., 2009), it was expected that the influence of the SOA from the boundaries over the domain would significantly affect not only the adjacent areas, but also Central Europe. Model differences between the baseline simulation and a configu-

ACPD
12, 21815–21865, 2012

ration using zero SOA concentration at the boundaries (scenario 2) quantify this effect, and are discussed in Sect. 4.4.1.

A model inter-comparison is presented in Sect. 4.4.2., and is two-fold: a SOA module inter-comparison is performed, in order to quantify and explain the differences in OA concentration predictions between the SORGAM (scenario 3) and the VBS approach (base-case). Comparisons are presented for the site of Cabauw (Netherlands). Then, an OA predictions inter-comparison is presented against results by the air quality model PMCAMx during the same period. Description of this model can be found in several publications (Environ, 2004; Karydis et al., 2010; Fountoukis et al., 2011), while organic aerosol chemistry is treated by a VBS version, analytically described in Tsimpidi et al. (2010). The PMCAMx application for May 2008 covers approximately the same area as the COSMO-ART application, but the horizontal resolution is coarser (36 km) and the vertical extent is shallower (14 vertical layers covering approximately 6 km height). The depth of the surface layer is 55 m. Meteorological fields are provided by offline WRF simulations, since PMCAMx is a chemical transport model. Anthropogenic, biogenic, sea-salt and wildfire emissions are provided by different sources/models than for COSMO-ART, as explained in Fountoukis et al. (2011). Boundary conditions for gaseous and aerosol pollutants are constant in space and time and, in case of secondary species, similar to COSMO-ART prescriptions. The first two days of the simulated period are again used as the model's spin up. The main differences to the COSMO-ART and VBS coupling, is that in PMCAMx primary organics are aged ($k = 4 \times 10^{-11}$ cm^{3}mol^{-1}s^{-1}), the rate constant used for anthropogenic SOA is higher ($k = 1 \times 10^{-11}$ cm^{3}mol^{-1}s^{-1}), and SOA of biogenic origin are not aged.

Other uncertain inputs to the model include the aging rate of SOA precursors along with the vaporization enthalpy. In order to bound the model predictions for plausible ranges of these parameters, a sensitivity study (scenario 4) is conducted using a faster and commonly used aging rate of $k = 1 \times 10^{-11}$ cm^{3}mol^{-1}s^{-1} (Murphy and Pandis, 2009, 2010; Farina et al., 2010; Fountoukis et al., 2011). This is coupled to a vaporization enthalpy commonly applied to VBS modules ($\Delta H_{vap} = 30$ kJ mol^{-1}), as it was

ACPD
12, 21815–21865, 2012

formerly found sufficient for reproducing smog chamber studies (Lane et al., 2008). The application of the currently used aerosol yields is also tested against lower values (scenario 5), occurring in a high-NO_x regime (Murphy and Pandis, 2009). This configuration is based upon the aforementioned k and ΔH_{vap} values, in order to estimate the overall sensitivity of the set of constants applied in the base-case simulation. The comparative results for OA are presented in Sect. 4.4.3.

The chemical aging of SOA in the atmosphere can act as a sink of hydroxyl radicals. Thus, by incorporating this procedure into modeling, Secondary Inorganic Aerosol (SIA) production is also expected to be influenced. Changes in the sum of sulfate, nitrate and ammonium aerosol (the main constituents of SIA) due to SOA oxidation are presented in the Sect. 4.4.4, after applying the model with aging not regarded as a net sink for OH (scenario 6).

Finally, the contribution of biogenic VOC sources on OA concentrations over Europe is estimated from aerosol differences between the baseline scenario and a simulation (scenario 7) excluding biogenic VOCs oxidation from being a SOA source (Sect. 4.4.5).

3.2 Measurements

During May 2008 an intensive measurement campaign was performed in Europe as part of the EUCAARI project (Kulmala et al., 2011). In the framework of the current study, model results are compared with hourly mean values from four measurement ground sites: Cabauw (Netherlands), Finokalia (Greece), Mace Head (Ireland) and Melpitz (Germany). All observation sites are not directly influenced by local sources, thus are representative of a regional pollution (Fig. 1).

The Cabauw site (51.971° N, 4.927° E) is located in a rural, agricultural region. The site provided measurements for total OA, sulfates: SO_4, NO_3 and ammonium: NH_4 mass for the period of 3 to 29 May 2008. The instrument used was a HR-ToF-AMS (Morgan et al., 2010b). The Finokalia sampling station (35.33° N, 25.67° E) is located at a remote, coastal area in the Eastern Mediterranean. The species measured are the same as in Cabauw, but the period available is shorter (8 to 29 May 2008). The instru-

ACPD
12, 21815–21865, 2012

ment used was a Q-AMS (Hildebrandt et al., 2010). Atmospheric temperature, humidity, wind and radiation are also available for the same period. Mace Head (53.32° N, 9.88° W) is a coastal atmospheric research station representative for studying long-range transport from the East of Europe. A HR-ToF-AMS was used to measure mass concentrations of organics during 23 to 29 May 2008. The site in Melpitz (12.93° E, 51.54° N) is located in flat, agricultural land and can be regarded as representative of the regional Central European aerosol. Data (from a HR-ToF-AMS) are available for total OA mass during the period of 23 May to 9 June 2008. Atmospheric temperature, humidity, wind, radiation, pressure and precipitation are also available for the same period.

3.3 Description of meteorology

The meteorological regime of May 2008 over Europe has been presented in several publications (Morgan et al., 2010a, b; Pikridas et al., 2010; Hamburger et al., 2011). Hereafter, a general description relevant to the current study is given.

The first half of May was dominated by an anticyclone blocking event, centered mainly over the Benelux states, the northern part of Germany and Denmark. Starting from 12 May, high pressure conditions prevailed over the North East Atlantic and the Central and Eastern Continental Europe. This regime lasted until 16 May and combined with the pathway of cyclones over Southern Europe resulted in a westward transportation of continental air masses towards Northwestern Europe. During 16 to 18 May, a trough evolved over Central Europe. Frontal systems associated with the trough changed the flow regime from westward to eastward air mass transport. Arctic air masses were advected via the North Sea towards continental Europe. The flow regime over Central Europe changed again its direction beginning on 18 May with the onset of an anticyclonic north-easterly pattern. Wind directions over Central Europe turned back to east after 21 May. During 19 to 21 May, a Saharan dust event was observed in Southern Europe.

ACPD
12, 21815–21865, 2012

4 Results

The modeling results are presented in four subsects.. First, representative hourly OA concentration fields are presented and analyzed along with the online wind field predictions and observational findings from previous studies (Sect. 4.1). Then, OA predictions are evaluated against ground measurement data, while a model inter-comparison is also performed (Sect. 4.2). Section (4.4) provides insights into the direct radiative effects related to SOA chemistry over Europe for May 2008. In order to investigate further SOA chemistry, a discussion on model outputs from the sensitivity studies described in Sect. 3.1 is given in Sect. 4.4.

4.1 Simulated OA concentrations

OA concentrations are found delocalized from their emission areas during the whole simulation period. This is because VOCs emissions are advected and aged downwind towards SOA. Aircraft measurements of more oxidized and less freshly OA during May 2008 (Morgan et al., 2010b) are also indicative of the photochemical processing of the OA over Europe, as predicted by COSMO-ART.

The aforementioned anticyclonic conditions over Central Europe are clearly reproduced by the current simulation and cause OA accumulation within the anticyclone (Fig. 2a). Pollution peaks inside the boundaries of the anticyclone are linked to the absence of clouds and precipitation and the inhibition of mixing of particles from the boundary layer into the free troposphere (Hamburger et al., 2011). Maximum hourly OA values reach 10 $\mu g\,m^{-3}$ during this blocking event.

After 12 May, when the anticyclone is formed over North East Atlantic, European continental air masses are transported westerly and lead to a pollution event over the Atlantic Ocean (Fig. 2b). Hourly OA concentrations over this area are well above 5 $\mu g\,m^{-3}$.

The change in the wind field during 16 to 18 May (Sect. 3.3), caused an advection of clean air masses (hourly OA mass values less than 1 $\mu g\,m^{-3}$) via the North Sea

ACPD
12, 21815–21865, 2012

towards continental Europe. This flow is already stated in Hamburger et al. (2011) and successfully represented by COSMO-ART (Fig. 2c). The northwestern transport of OA towards the Eastern Mediterranean during the same period confirms its origin from continental Greece, as calculated with the particle dispersion model FLEXPART (Pikridas et al., 2010). According to measurement analysis of Hildebrandt et al. (2010), OA was diluted and highly aged by the time air masses reached Finokalia. This explains the elevated OA predictions over the sea (hourly values more than $5\,\mu g\,m^{-3}$) when compared to the less processed air masses over continental Greece (hourly values less than $5\,\mu g\,m^{-3}$).

This event was followed by an Africa air mass intrusion (19 to 21 May) (Pikridas et al., 2010). Predictions by COSMO-ART confirm this flow regime, which is accompanied with low OA values (up to $1\,\mu g\,m^{-3}$), because aerosol transport from Africa is not represented by the current application (Fig. 2d). A detailed study on this event as simulated by COSMO-ART is recently published (Bangert et al., 2012).

The change of wind direction to east after 21 May over Central Europe led to an increase in concentrations over Northwestern Europe (Hamburger et al., 2011). The above is realistically predicted by the simulation (hourly OA mass values of 5 to $10\,\mu g\,m^{-3}$) (Fig. 2e). From then on, the wind field over Central Europe becomes weaker, and its eastern component transfer air masses from Poland towards Germany (Fig. 2f). OA levels within these aerosol masses reach $10\,\mu g\,m^{-3}$. The strong influence of long-range transport of secondary particle masses from the east is systematically observed over this area (Spindler et al., 2010).

The geographical distribution of monthly mean OA produced by this study (Fig. 3) is compared to earlier model results over Europe that applied VBS. For most parts of Europe, the calculated total OA in fine particles both by EMEP (Bergström et al., 2012) and COSMO-ART (current study) is around 2–3 $\mu g\,m^{-3}$, while PMCAMx (Fountoukis et al., 2011) results in lower values (1.5 to $2\,\mu g\,m^{-3}$). Another similarity between the current study and EMEP outputs is the elevated OA values over the Mediterranean area, when compared to lower PMCAMx results. Nevertheless, similar OA peaks are

ACPD
12, 21815–21865, 2012

predicted by PMCAMx and COSMO-ART over the English Channel, which are not shown in EMEP results. Overall, OA differences among the three simulation studies are not significant. Since the study by Bergström et al. (2012) does not include the year 2008, a direct comparison with the results of the current study is not possible, but PMCAMx results are incorporated to the Sect. 4.4.2.

4.2 OA performance of COSMO-ART

While the previous paragraph largely proves the model's efficiency to qualitatively reproduce the atmospheric circulation observed over the whole European area during May 2008, this section is an attempt to evaluate local OA predictions in a quantitative manner. For this reason, the time series of the total PM_1 organic matter measured and predicted by COSMO-ART during the EUCAARI May 2008 campaign is presented in Fig. 4 and monthly mean values together with performance metrics lie in Table 4.

Average PM_1 organic aerosol measurements are around 5.1 and 4.2 $\mu g\,m^{-3}$ for the Central European sites in Germany and the Netherlands, respectively, while the peripheral sites of Finokalia and Mace Head exhibit lower values (3.1 and 1.3 $\mu g\,m^{-3}$, respectively). Similar are the prediction findings (4.3, 3.6, 2.5 and 2.4 $\mu g\,m^{-3}$, respectively). The prediction skill of COSMO-ART PM_1 OA mass is quantified in terms of the Mean Fractional Bias (MFB) and Mean Fractional Error (MFE) metrics (Boylan and Russell, 2006). The equations for MFB and MFE are:

$$\mathrm{MFB} = \frac{1}{N}\sum_{i=1}^{N}\frac{(C_\mathrm{m} - C_\mathrm{o})}{\left(\frac{C_\mathrm{o}+C_\mathrm{m}}{2}\right)}, \quad (1)$$

$$\mathrm{MFE} = \frac{1}{N}\sum_{i=1}^{N}\frac{|C_\mathrm{m} - C_\mathrm{o}|}{\left(\frac{C_\mathrm{o}+C_\mathrm{m}}{2}\right)}, \quad (2)$$

where C_m is the modeled and C_o is the observed hourly value for the total PM_1 OA concentration ($\mu g\,m^{-3}$) at the site i of N.

ACPD
12, 21815–21865, 2012

According to the proposed model performance goal (MFE ≤ +50 % and MFB ≤ ±30 %) and criteria (MFE ≤ +75 % and MFB ≤ ±60 %), the level of accuracy of COSMO-ART predictions for OA over all sites is the best a model can be expected to achieve (goal is met). Separately, OA predictions for Mace Head, Finokalia and Melpitz are acceptable (criteria is met), while Cabauw performs at the best level of accuracy (goal is met).

Overall, both the hourly and the diurnal variation of organics are well captured by the model at all four aforementioned sites. Specifically, the observed daily cycle of OA over Cabauw (Fig. 4a) is successfully reproduced, and shows an increase during afternoon due to the photochemical aging of aerosol combined to mixing of aged OA from aloft and a peak during nighttime due to partitioning from gas to particle phase, being maximized at a lower mixing height and temperature. During the first half of May and due to the anticyclonic event, polluted air masses are predicted to be transported towards Cabauw from North Germany (Fig. 2a), which is consistent with the calculated air mass trajectories using the ECMWF wind field (Hamburger et al., 2011). The low OA concentrations observed and predicted during 16 to 21 May are caused by the transport of Arctic masses towards Europe (Fig. 2c). Long-range transport of masses from Central Europe causes an increase in OA concentrations from the 21st of May and on.

A common feature of predictions and observations over Finokalia is the absence of a clear daily cycle of OA (Fig. 4b). This is due to the lack of local or nearby sources of OA. The highest OA concentrations occur around the middle of the month and originate from Athens and the rest of continental Greece (Fig. 2c). During this period, lower wind speeds are predicted and observed (Pikridas et al., 2010). This leads to an increased accumulation of organics in the atmosphere, which are intensively aged and added to the next day's SOA formation. This episode is captured though over-predicted by COSMO-ART. The Africa air mass intrusion that follows (20 to 21 May) leads to OA underestimation. According to Hildebrandt et al. (2010), the air mass transported from the south was possibly influenced by major cities in Africa, thus containing quite fresh

ACPD
12, 21815–21865, 2012

and not aged OA. This organic content of aerosol is not represented by the boundary conditions applied in the current simulations (Sect. 3.1). Further, emissions from African countries are not included in the inventory used in these simulations.

The diurnal variation of organics is moderately reproduced over Mace Head (Fig. 4c). A noticeable underestimation occurs during 16 to 17 May, when air masses arrive to Mace Head from the northeast (Hamburger et al., 2011). COSMO-ART shows that northeastern wind directions transfer organic-free air masses from the North Sea and the Scandinavian Peninsula (Fig. 2c). This could be related to a currently unidentified VOC source by the emission inventory used. Elevated OA masses from 23 until 26 May are shown both in measurements and model and originate from pollution sources at the continental Europe (Fig. 2e).

Noticeable discrepancies between hourly OA predictions and observations occur over Melpitz (Fig. 4d). Although northeastern winds over Central Europe (Hamburger et al., 2011) are found to cause high levels of OA over Melpitz on 24 May, predictions show that these winds transfer clean air masses towards Germany, Poland and the Czech republic during the same period (Fig. 2e). OA model results are much lower than measurements during this event, implying again a possible real source of organics missing from the emission databases used, at European Russia north of Moscow. OA peaks after 26 May represent air masses transported from Eastern Europe, usually underestimated by chemical transport models (Spindler et al., 2010). Nevertheless, COSMO-ART succeeds to reproduce the high OA values measured, but the strong spatial gradient of the predicted field (Fig. 2f), makes the effect of point-to-grid comparison stronger and their temporal correlation weaker.

Oxygenated organic aerosol is predicted to be 80 to 95 % of the total PM_1 organics, which is in line with measurement studies (Zhang et al., 2007; Morgan et al., 2010b; Hildebrandt et al., 2010). This shows the preponderance of atmospheric chemical transformations of organic matter over the freshly emitted organic aerosol. More analytically, measurements during May 2008 over Europe (Morgan et al., 2010b) indicate that POA typically contributes 5 to 20 % to the regional OA burden. According to mea-

ACPD
12, 21815–21865, 2012

surements of Hildebrandt et al. (2010), HOA at Finokalia was not present in detectable amounts. Likewise, COSMO-ART calculated the minimum POA amount of OA (5 %) over this site. The reproduction of this finding by COSMO-ART, supports the efficiency of the currently applied VBS version, which treats SOA, but not POA, as chemically active. This is strengthened by Zhang et al. (2007) measurements, which concluded that HOA oxidation is not an important source of OOA, and that OOA increases are mainly due to SOA.

4.3 SOA direct radiative effect

The average changes on aerosol and its feedback, which are imposed by SOA simulated by the VBS scheme applied over Europe (base-case scenario) are depicted in Table 5. SOA is the major component of the additional aerosol mass (approximately $2\,\mu g\,m^{-3}$). The latter corresponds to more than 55 % of total PM_1 predictions by the baseline simulation. Besides SOA, 5 % of this mass corresponds to increased sulfate and ammonium formation (nitrate mass is found negligible). This surplus to aerosol originates from the enhanced condensation onto a larger aerosol surface due to the organic mass, and results in an increase in the mean diameter of aerosol. This is expressed though the 5 % increase in the accumulation fraction of total PM_1. As a consequence, water uptake by aerosol is also enhanced (5 %). These mass and size changes in aerosol influence the degree of light transmission that is prevented, which is expressed through a moderate increase of aerosol optical depth, which corresponds to almost 15 % of the total AOD. As the aerosol scattering increases due to organics, sulfates, ammonium and water, the reflection of solar radiation back to space is also increased. The effect on the long wave radiation back to earth is much weaker, thus the net surface radiative forcing imposed by organic aerosol chemistry is negative. The predicted mean direct surface radiative cooling averaged over Europe is $-1.2\,W\,m^{-2}$ for May 2008 and contributes approximately by 20 % to the total aerosol effect. Over certain areas (e.g. Southeastern Germany, Fig. 5) the predicted radiative cooling is an order of magnitude stronger than the mean value of $-1.2\,W\,m^{-2}$. The corresponding

ACPD
12, 21815–21865, 2012

decrease in average temperature (at 2 m altitude) is calculated at −0.1 K, which is small though reflects almost 60 % of total aerosol forcing predictions. Maximum values of surface temperature decrease reach −0.3 K (e.g. over European Russia).

These values correspond to a polluted period compared to the rest of 2008 (Morgan et al., 2010b). Moreover, they are the response to the forcing applied within the European area, but following Shindell and Faluvegi (2009) findings for black carbon and sulfates, forcing linked to organic aerosol mass over the tropics and the arctic is also expected to contribute to the total surface air temperature changes over Europe.

Simulations on the global scale have shown an annual mean SOA radiative cooling over Europe in the range of −0.25 to −0.75 $W m^{-2}$, when organic mass is predicted up to 2 $\mu g m^{-3}$, which is much lower than the measured values (up to 6 $\mu g m^{-3}$) (Ming et al., 2005; Myhre et al., 2009; O' Donnell et al., 2011). To the best of our knowledge there do not exist any other publications on SOA direct radiative forcing over Europe on the regional scale. Nevertheless, the results of the current study are in line with the yearly averaged anthropogenic aerosol feedback over Europe ($\Delta sR = -1$ to $-3\,W m^{-2}$ and $\Delta T = -0.1$ to −0.2 K), as calculated by a regional model (Zanis et al., 2012).

It should be pointed out that the SOA-imposed direct radiative forcing is caused not only by aerosol scattering radiation, but also partially by the semi-direct effect of cloud cover, which was abundant in the simulation period (Fig. 3b). Cloud cover is modified by the aforementioned total aerosol changes and in turn affects aerosol radiative forcing. Although the sum of cloud cover over Europe is predicted nearly unaffected by SOA chemistry (Table 5), the model gives a noisy result for its spatial distribution (Fig. 5a). Contrary to the average regime described in the previous paragraph, in areas where the decrease of cloud cover reaches up to 5 %, short and long wave radiative forcings reach their highest (+13 $W m^{-2}$) and lowest values (−4 $W m^{-2}$), respectively (Fig. 5b, c). These areas cover approximately 30 % of the European domain, where a monthly average temperature increase of 0.2 K (at 2 m altitude) is predicted (Fig. 5d).

ACPD
12, 21815–21865, 2012

4.4 Sensitivity analysis

The results and analysis that follow are based on the scenarios 2 to 7 presented in Table 3 and described in Sect. 3.1.

4.4.1 Impact of boundary conditions

The OA that is transported into the European area from the boundaries of the modeling domain is shown in Fig. 6 for the four selected sites (grey dashed line). Their monthly average concentration is around 1 $\mu g\,m^{-3}$, which is the value set at the boundaries of the domain. This value represents an important fraction of total OA, thus influences OA predictions.

25 % of the total OA over the Central European sites (Cabauw and Melpitz) is attributed to the effect of the boundary conditions. During the northern wind conditions (16 to 21 May), which transfer clean air masses towards Central Europe and disperse local pollution, the role of boundary conditions is maximized over Cabauw. Mace Head is the site that is influenced the most by the boundary OA concentrations (66 %), due to its proximity to the western edge of the domain. During the last days of the month, there seems to be an equal contribution of European pollution and the background situation on OA over Mace Head.

Although Finokalia is also relatively close to the borders of the domain, the calculated effect of the boundaries on OA is the half than over Mace Head (33 %). This is attributed to the high photochemical activity in Southern Europe, which strengthens the role of chemical oxidation and regional SOA formation and to a much stronger predominance of westerly flow patterns in Mace Head.

4.4.2 Model inter-comparison

The OA outputs from scenario 3 (SORGAM approach) are compared against the base-case COSMO-ART simulation (VBS approach) in respect to observations. As evident,

ACPD
12, 21815–21865, 2012

SORGAM reproduces the daily cycle in Cabauw (orange line in Fig. 6). This was expected, as gas-to-particle mass transfer is similar in both SOA modules. Nevertheless, significant deviations from the baseline scenario and measurements occur around noon and midnight hours, when scenario 3 reaches unrealistically low values. During daytime, this deficit reflects the inability of SORGAM to treat the photochemical aging of SOA. Subsequently, the background aged SOA concentrations during nighttime are also missing from scenario 3 predictions. On average (3 to 10 May), OA is measured to be 4 $\mu g\,m^{-3}$ over Cabauw, while COSMO-ART gives low values with SORGAM (2.7 $\mu g\,m^{-3}$), in contrast to the realistic results produced by VBS (4.1 $\mu g\,m^{-3}$). The corresponding values for Mace Head and Melpitz are 1.5 (scenario 3), 2.4 (base-case) and 2.2 (scenario 3), 2.8 $\mu g\,m^{-3}$ (base-case), respectively. The biggest differences exhibit in Finokalia, due to the increased photochemical activity and SOA aging, which is not simulated by scenario 3 (0.8 $\mu g\,m^{-3}$) in contrast to the base-case simulation (2.2 $\mu g\,m^{-3}$). Significant deviations from OA observations also exist in WRF-CHEM applications bound to the SORGAM module, applied over the Eastern United States (Ahmadov et al., 2012).

COSMO-ART to PMCAMx inter-comparison on organic aerosol predictions (green and blue line in Fig. 6, respectively) reveals neither large nor systematic differences. Sources of discrepancies are differences in the spatial resolution of models, emission databases applied, meteorology (online-calculated and hourly inputs from the meteorological model WRF, respectively) and differences in the chemical oxidation of organic matter. The latter is related to the lower aging constant rates used by COSMO-ART, and the absence of aging the biogenic VOCs in PMCAMx.

These differences counteract, and are most probably the reason for the non-systematic behavior of OA results. Nevertheless, common model behavior supports some aforementioned arguments (Sect. 4.2). In specific, northeastern winds towards Mace Head (16 to 17 May) and Melpitz (24 May) contribute to low PMCAMx OA predictions, similarly to COSMO-ART, and strengthen the argument of poor emission representation over North Sea, Scandinavian Peninsula and at European Russia North of

ACPD
12, 21815–21865, 2012

Moscow. In addition, the underestimation of OA levels over Finokalia during the Africa event (20 to 21 May) shows that under certain conditions African cities can be an important source of OA mass poorly represented by modeling over Europe, unless nested into an extended domain towards the south.

4.4.3 SOA formation and constant parameters

Figure 6 shows OA concentrations by two additional simulations (scenarios 4 and 5), after modifying the aging constants as described in Sect. 3.1. OA predictions by scenario 4 (red line in Fig. 6) are in general a lot higher than observations and baseline results, mainly because of the higher aging constant applied. These differences are maximized upon OA peaks (e.g high values during 5 to 15 May over Cabauw) and are minimized when OA values are low and close to background levels. The most unrealistic OA peaks predicted by this scenario occur over Finokalia and Melpitz. This is because, as aforementioned, both sites are situated within a greater area of high-OA regime, resulting from the increased photochemical activity and from eastern transport, respectively. In conclusion, under such conditions total OA concentrations are controlled by the assumed oxidation rates of SOA.

The above shows that this configuration is not as appropriate for Europe as the base-case one. Mace Head represents an exception: the monthly average increase from this scenario is small ($0.5\,\mu g\,m^{-3}$), but results in MFE = +38 % and MFB = −30 %, thus to the highest accuracy a model can reach according to Boylan and Russell (2006).

In order to investigate whether the unrealistic peaks stem from overestimated aerosol yields applied for VOCs, this scenario is compared to scenario 5 (yellow line in Fig. 6). As expected, SOA values are decreased in comparison to scenario 4, but not more than 10 %. Thus, the dependence of aerosol yields on the NO_x regime does not influence significantly OA predictions in this case. These findings strengthen the arguments for the importance of the chemical aging of SOA in comparison to the initial formation/stage in the atmosphere.

ACPD
12, 21815–21865, 2012

4.4.4 SOA aging and inorganic chemistry

The main effect of OH consumption during SOA oxidation is the decreased production of nitric and sulfuric acids from NO_2 and SO_2 oxidation, respectively. The decreased availability of acids in the atmosphere, leads to decreased levels of sulfate, nitrate and ammonium and leaves more NH_3 in the gas phase. This chemical regime is depicted by calculating the sign of differences of the aforementioned species as predicted by the base-case simulation and by the scenario 6. Although values are small when averaged for an 8-day period over Europe (Fig. 7), they reach around -0.5, -3 and $-1\,\mu g\,m^{-3}$ on an hourly basis for sulfate, nitrate and ammonium, respectively, in a high-NO_x regime. This decrease due to SOA formation corresponds to the 5 to 30 % of hourly SIA base-case concentrations.

SIA performance of COSMO-ART after incorporating SOA aging through the VBS scheme is found optimal. In specific, mean monthly SIA measurements and predictions over Cabauw are 5 and $5.2\,\mu g\,m^{-3}$, respectively, while for Finokalia both values are $4\,\mu g\,m^{-3}$. Since the number of values compared here is relatively small (117 and 55, respectively), this evaluation is only indicative and not representative for secondary inorganic aerosol performance with COSMO-ART. Nevertheless, a detailed study towards this direction (Knote et al., 2011) showed nitrate overestimation, which is the specie found here mostly decreased due to SOA aging. This indicates that the current version of COSMO-ART has improved performance not only in organic, but also in inorganic aerosol, which needs further investigation during an event with enough SIA measurements.

4.4.5 Anthropogenic and biogenic SOA sources

Figure 8 shows the average SOA mass in PM_1 concentration (a), its predicted biogenic fraction (b) and average concentrations of anthropogenic (c) and biogenic (d) VOCs (precursor species are shown in Table 1). Over a large part of the simulation domain

ACPD
12, 21815–21865, 2012

biogenic SOA are the dominant OA component. This fraction reflects nonurban sources not explicitly included in the model.

Peak SOA concentrations over the latitudinal zone of continental Europe from 40 and 55 deg N (Fig. 8a) originate mainly from biogenic VOCs, although not above 60 % (Fig. 8b). The atmospheric chemical analysis of aircraft measurements during May 2008 (Morgan et al., 2010b) is also suggestive of the anthropogenic influence on oxygenated organic aerosol over Europe. However, that study lacks suitable information regarding gas-phase organic precursors, which is attempted here (Fig. 8c, d). COSMO-ART results show that the sum of the anthropogenic SOA precursors significantly outweighs biogenic VOCs concentrations. This is mainly reflected over the Mediterranean Sea, where the former is significantly greater than the latter. The maximum influence of anthropogenic VOCs over the Mediterranean Sea is also shown from predictions by Bergström et al. (2012) over Europe.

5 Conclusions

Use of the Volatility Basis Set approach (VBS) to simulate Secondary Organic Aerosol (SOA) formation over Europe led to improved organic aerosol predictions by the regional atmospheric model COSMO-ART and allowed investigation of their impact upon the radiative budget during May 2008.

Atmospheric circulation and air pollution transport as predicted by COSMO-ART are consistent with observations (Pikridas et al., 2010; Hildebrandt et al., 2010; Hamburger et al., 2011), which further allows for the estimation of accuracy of organic aerosol treatment and representation within the model.

The delocalization of organic aerosol from its sources exhibits throughout the whole simulation period and reflects their transport and chemical oxidation towards highly condensable species. This is in line with the high secondary to total organics ratio (80 to 95 %) all over the European area for the May period. These physicochemical processes shape the monthly mean surface organic aerosol concentrations from 2.5

ACPD
12, 21815–21865, 2012

to 4.5 $\mu g\,m^{-3}$ over most European areas. Higher SOA values are predicted to originate mainly from biogenic activities, though anthropogenic influence is important (around 40 %), as previously suggested by simultaneous aircraft measurements (Morgan et al., 2010b).

Comparison of hourly predictions with point measurements in the framework of the EUCAARI campaign shows that COSMO-ART meets the performance goals for total organic aerosol mass, as defined by Boylan and Russell (2006). This indicates that the significant reduction of surrogate species applied in the current version of VBS scheme provides COSMO-ART with both speed and accuracy.

Interactive coupling performed by COSMO-ART enables the estimation of SOA interaction with radiation on a regional scale. Results in this study show a mean monthly-average direct radiative forcing around $-1.2\,W\,m^{-2}$, imposed by SOA chemistry at the surface over Europe during May 2008, which is followed by a small decrease in temperature (−0.1 K). Nevertheless, responses are not spatially correlated with the forcing, due to the nonlinearity involved in the feedbacks among major processes. Cloud cover modifications, due to changes in particle chemical composition, water content and size distribution, result even in a positive radiative forcing, though over a limited surface. This semi-direct phenomenon is also responsible for the greater global and local sensitivities to forcing (Shindell and Faluvegi, 2009). Therefore, the surface air temperature changes calculated in the current study correspond to the regional contribution of forcing imposed by SOA concentrations on the global scale.

Results from the sensitivity simulations related to the secondary organic chemistry modules revealed important information related to their treatment within atmospheric models. The inability of SORGAM to treat the chemical oxidation of organic matter leads to an underestimation of 35 % of OA against VBS predictions and measurements. Sensitivity tests on the parameters used within the VBS approximation showed that NO_x availability causes small differences in SOA production, but the aging rate constant should be carefully selected.

ACPD
12, 21815–21865, 2012

By combining local findings with hourly wind and mass fields over Europe, as predicted by COSMO-ART, the origin of organic aerosol peaks is identified. Elevated hourly organic aerosol values (4 to 10 $\mu g\,m^{-3}$) over Cabauw, Mace Head and Melpitz occur during air mass transport from the east towards these areas, while northeastern wind directions cause high values over Finokalia. Total organic aerosol concentration predictions are significantly affected by the boundary concentrations assumed in the model. In specific, 25 % of total organic aerosol predictions in the Central European area corresponds to background concentrations, and increases near the edges of the domain.

The inter-comparison of COSMO-ART and PMCAMx against measurements can help towards identifying possible sources for model discrepancies. Organic aerosol underestimations commonly found by both models during northeastern winds over Mace Head and Melpitz are possibly caused by unidentified sources of organic precursors at the Scandinavian Peninsula and in Northern European Russia.

The effort to improve COSMO-ART organic aerosol predictions, which was addressed by Knote et al. (2011), is proven to be critical not only for organics, but also for the overall COSMO-ART aerosol performance. In specific, SOA aging is found to reduce nitrate production up to 30 % on an hourly basis, while the condensation upon pre-existing particles including secondary organics, results in a monthly average increase of 5 % in sulfate and ammonium formation in the accumulation mode. Thus, one of the sources of nitrate overestimation and sulfate underestimation found by Knote et al. (2011) is now eradicated from COSMO-ART chemistry. The consistency of secondary inorganic aerosol predictions with observations in the framework of this study is a first indication towards this conclusion.

Future research is focused on a cloud-free case of an OA episode towards the identification of a clear correlation between aerosol concentration and radiative fluxes. The indirect impact of condensing organics is included in further model development.

Acknowledgements. The authors would like to thank A. Mensah, A. Kiendler-Scharr, M. Dall'Osto, C. O'Dowd and L. Poulain concerning EUCAARI data.

ACPD
12, 21815–21865, 2012

The service charges for this open access publication have been covered by a Research Centre of the Helmholtz Association.

References

Ackermann, I., Hass, H., Memmesheimer, M., Ebel, A., Binkowski, F., and Shankar U.: Modal aerosol dynamics model for Europe: development and first applications, Atmos. Environ., 32, 2981–2999, 1998.

Ahmadov, R., McKeen, S. A., Robinson, A. L., Bahreini, R., Middlebrook, A. M., de Gouw, J. A., Meagher, J., Hsie, E.-Y., Edgerton, E., Shaw, S., and Trainer, M.: A volatility basis set model for summertime secondary organic aerosols over the Eastern United States in 2006, J. Geophys. Res., 117, 06301, doi:10.1029/2011JD016831, 2012.

Andersson-Sköld, Y. and Simpson, D.: Secondary organic aerosol formation in northern Europe: A model study, J. Geophys. Res., 106, 7357–7374, doi:10.1029/2000JD900656, 2001.

Baeumer, D., Lohmann, U., Lesins, G., Li, J., and Croft, B.: Parameterizing the optical properties of carbonaceous aerosols in the canadian centre for climate modeling and analysis atmospheric general circulation model with impacts on global radiation and energy fluxes, J. Geophys. Res., 112, 10207, doi:10.1029/2006JD007319, 2007.

Bahreini, R., Ervens, B., Middlebrook, A. M., Warneke, C., de Gouw, J. A., DeCarlo, P. F., Jimenez, J. L., Brock, C. A., Neuman, J. A., Ryerson, T. B., Stark, H., Atlas, E., Brioude, J., Fried, A., Holloway, J. S., Peischl, J., Richter, D., Walega, J., Weibring, P., Wollny, A. G., Fehsenfeld, F. C.: Organic aerosol formation in urban and industrial plumes near Houston and Dallas, Texas, J. Geophys. Res., 114, D00F16, doi:10.1029/2008JD011493, 2009.

Baldauf, M., Seifert, A., Förstner, J., Majewski, D., Raschendorfer, M., and Reinhardt, T.: Operational convective-scale numerical weather prediction with the COSMO model: description and sensitivities, Mon. Weather Rev., 139, 3887–3905, doi:10.1175/MWR-D-10-05013.1, 2011.

Bangert, M., Kottmeier, C., Vogel, B., and Vogel, H.: Regional scale effects of the aerosol cloud interaction simulated with an online coupled comprehensive chemistry model, Atmos. Chem. Phys., 11, 4411–4423, doi:10.5194/acp-11-4411-2011, 2011.

ACPD

12, 21815–21865, 2012

Bangert, M., Nenes, A., Vogel, B., Vogel, H., Barahona, D., Karydis, V. A., Kumar, P., Kottmeier, C., and Blahak, U.: Saharan dust event impacts on cloud formation and radiation over Western Europe, Atmos. Chem. Phys., 12, 4045–4063, doi:10.5194/acp-12-4045-2012, 2012.

Bartholomé, E. and Belward, A. S.: GLC2000: a new approach to global land cover mapping from Earth observation data, Int. J. Remote Sens., 26, 1959–1977, 2005.

Bergström, R., Denier van der Gon, H. A. C., Prévôt, A. S. H., Yttri, K. E., and Simpson, D.: Modelling of organic aerosols over Europe (2002–2007) using a volatility basis set (VBS) framework with application of different assumptions regarding the formation of secondary organic aerosol, Atmos. Chem. Phys. Discuss., 12, 5425–5485, doi:10.5194/acpd-12-5425-2012, 2012.

Bessagnet, B., Menut, L., Curci, G., Hodzic, A., Guillaume, B., Liousse, C., Moukhtar, S., Pun, B., Seigneur, C., and Schulz, M.: Regional modeling of carbonaceous aerosols over Europe-focus on secondary organic aerosols, J. Atmos. Chem., 61, 175–202, doi:10.1007/s10874-009-9129-2, 2008.

Bohren, C. F. and Huffman, D. R.: Absorption and Scattering of Light by Small Particles, Wiley, New York, 1983.

Boylan, J. and Russell, A.: PM and light extinction model performance metrics, goals, and criteria for three-dimensional air quality models, Atmos. Environ., 40, 4946–4959, doi:10.1016/j.atmosenv.2005.09.087, 2006.

Carslaw, K. S., Boucher, O., Spracklen, D. V., Mann, G. W., Rae, J. G. L., Woodward, S., and Kulmala, M.: A review of natural aerosol interactions and feedbacks within the Earth system, Atmos. Chem. Phys., 10, 1701–1737, doi:10.5194/acp-10-1701-2010, 2010.

Chen, Q., Farmer, D. K., Schneider, J., Zorn, S. R., Heald, C. L., Karl, T. G., Guenther, A., Allan, J. D., Robinson, N., Coe, H., Kimmel, J. R., Pauliquevis, T., Borrmann, S., Pöschl, U., Andreae, M. O., Artaxo, P., Jimenez, J. L., Martin, S. T.: Mass spectral characterization of submicron biogenic organic particles in the Amazon Basin, Geophys. Res. Lett., 36, L20806, doi:10.1029/2009GL039880, 2009.

Chuang, M.-T., Zhang, Y., and Kang, D.: Application of WRF/Chem-MADRID for real-time air quality forecasting over the Southeastern United States, Atmos. Environ., 45, 6241–6250, doi:10.1016/j.atmosenv.2011.06.071, 2011.

de Gouw, J. A., Middlebrook, A. M., Warneke, C., Goldan, P. D., Kuster, W. C., Roberts, J. M., Fehsenfeld, F. C., Worsnop, D. R., Canagaratna, M. R., Pszenny, A. A. P., Keene, W. C.,

ACPD
12, 21815–21865, 2012

Marchewka, M., Bertman, S. B., and Bates, T. S.: Budget of organic carbon in a polluted atmosphere: results from the new England air quality study in 2002, J. Geophys. Res., 110, D16305, doi:10.1029/2004JD005623, 2005.

de Gouw, J. A., Welsh-Bon, D., Warneke, C., Kuster, W. C., Alexander, L., Baker, A. K., Beyersdorf, A. J., Blake, D. R., Canagaratna, M., Celada, A. T., Huey, L. G., Junkermann, W., Onasch, T. B., Salcido, A., Sjostedt, S. J., Sullivan, A. P., Tanner, D. J., Vargas, O., Weber, R. J., Worsnop, D. R., Yu, X. Y., and Zaveri, R.: Emission and chemistry of organic carbon in the gas and aerosol phase at a sub-urban site near Mexico City in March 2006 during the MILAGRO study, Atmos. Chem. Phys., 9, 3425–3442, doi:10.5194/acp-9-3425-2009, 2009.

Donahue, N. M., Robinson, A. L., Stanier, C. O., and Pandis, S. N.: Coupled partitioning, dilution, and chemical aging of semivolatile organics, Environ. Sci. Technol., 40, 2635–2643, 2006.

Donahue, N. M., Epstein, S. A., Pandis, S. N., and Robinson, A. L.: A two-dimensional volatility basis set: 1. organic-aerosol mixing thermodynamics, Atmos. Chem. Phys., 11, 3303–3318, doi:10.5194/acp-11-3303-2011, 2011.

Dzepina, K., Volkamer, R. M., Madronich, S., Tulet, P., Ulbrich, I. M., Zhang, Q., Cappa, C. D., Ziemann, P. J., and Jimenez, J. L.: Evaluation of recently-proposed secondary organic aerosol models for a case study in Mexico City, Atmos. Chem. Phys., 9, 5681–5709, doi:10.5194/acp-9-5681-2009, 2009.

Elleman, R. A. and Covert, D. S.: Aerosol size distribution modeling with the community multiscale air quality modeling system in the Pacific Northwest: 1. Model comparison to observations, J. Geophys. Res., 114, D11206, doi:10.1029/2008JD010791, 2009.

Emmons, L. K., Walters, S., Hess, P. G., Lamarque, J.-F., Pfister, G. G., Fillmore, D., Granier, C., Guenther, A., Kinnison, D., Laepple, T., Orlando, J., Tie, X., Tyndall, G., Wiedinmyer, C., Baughcum, S. L., and Kloster, S.: Description and evaluation of the Model for Ozone and Related chemical Tracers, version 4 (MOZART-4), Geosci. Model Dev., 3, 43–67, doi:10.5194/gmd-3-43-2010, 2010.

ENVIRON: User's guide to the comprehensive air quality model with extensions (CAMx), version 5.40, report, available at: http://www.camx.com, Novato, CA, USA, 2011.

Farina, S. C., Adams, P. J., and Pandis, S. N.: Modeling global secondary organic aerosol formation and processing with the volatility basis set: implications for anthropogenic secondary organic aerosol, J. Geophys. Res., 115, D09202, doi:10.1029/2009JD013046, 2010.

ACPD
12, 21815–21865, 2012

Forster, P., Ramaswamy, V., Artaxo, P., Berntsen, T., Betts, R., Fahey, D. W., Haywood, J., Lean, J., Lowe, D. C., Myhre, G., Nganga, J., Prinn, R., Raga, G., Schulz, M., and van Dorland, R.: Changes in atmospheric constituents and in radiative forcing. in: Climate Change 2007: The Physical Science Basis. Contribution of Working Group I to the Fourth Assessment Report of the Intergovernmental Panel on Climate Change, edited by: Solomon, S., D. Qin, M. Manning, Z. Chen, M. Marquis, K. B. Averyt, M.Tignor and H. L. Miller. Cambridge University Press, Cambridge, UK and New York, NY, USA, 131–234, 2007.

Fountoukis, C. and Nenes, A.: ISORROPIA II: a computationally efficient thermodynamic equilibrium model for $K^+ - Ca^{2+} - Mg^{2+} - NH^{4+} - Na^+ - SO_4^{2-} - NO_3^- - Cl^- - H_2O$ aerosols, Atmos. Chem. Phys., 7, 4639–4659, doi:10.5194/acp-7-4639-2007, 2007.

Fountoukis, C., Racherla, P. N., Denier van der Gon, H. A. C., Polymeneas, P., Charalampidis, P. E., Pilinis, C., Wiedensohler, A., Dall'Osto, M., O'Dowd, C., and Pandis, S. N.: Evaluation of a three-dimensional chemical transport model (PMCAMx) in the European domain during the EUCAARI May 2008 campaign, Atmos. Chem. Phys., 11, 10331–10347, doi:10.5194/acp-11-10331-2011, 2011.

Geiger, H., Barnes, I., Bejan, I., Benter, T., and Spittler, M.: The tropospheric degradation of isoprene: an updated module for the regional atmospheric chemistry mechanism, Atmos. Environ., 37, 1503–1519, 2003.

Grell, G. A., Peckham, S. E., Schmitz, R., McKeen, S. A., Frost, G., Skamarock, W. C., and Eder, B.: Fully coupled "online" chemistry within the WRF model, Atmos. Environ., 39, 6957–6975, doi:10.1016/j.atmosenv.2005.04.027, 2005.

Hamburger, T., McMeeking, G., Minikin, A., Birmili, W., Dall'Osto, M., O'Dowd, C., Flentje, H., Henzing, B., Junninen, H., Kristensson, A., deLeeuw, G., Stohl, A., Burkhart, J. F., Coe, H., Krejci, R., and Petzold, A.: Overview of the synoptic and pollution situation over Europe during the EUCAARI-LONGREX field campaign, Atmos. Chem. Phys., 11, 1065–1082, doi:10.5194/acp-11-1065-2011, 2011.

Han, Z., Li, J., Xia, X., and Zhang, R.: Investigation of direct radiative effects of aerosols in dust storm season over East Asia with an online coupled regional climate-chemistry-aerosol model, Atmos. Environ., 54, 688–699, doi:10.1016/j.atmosenv.2012.01.041, 2012.

Herwehe, J. A., Otte, T. L., Mathur, R., and Rao, S. T.: Diagnostic analysis of ozone concentrations simulated by two regional-scale air quality models, Atmos. Environ., 45, 5957–5969, doi:10.1016/j.atmosenv.2011.08.011, 2011.

ACPD
12, 21815–21865, 2012

Hildebrandt, L., Lee, B., Kostenidou, E., Mohr, C., Engelhart, G. J., Tsimpidi, A., Karydis, V., deCarlo, P. F., Prevot, A. S. H., Baltensperger, U., Donahue, N. M., Mihalopoulos, N., and Pandis, S. N.: Origin, Composition and Volatility of Aerosol in the Eastern Mediterranean During the EUCAARI Intensive Campaign: the Finokalia Aerosol Measurement Experiment – 2008. EGU, European Geosciences Union General Assembly 2009, Vienna, Austria, 19–24 April, Abstr. No. T170A11, Carnegie Mellon University, Pittsburgh, PA, USA, 2009.

Hildebrandt, L., Engelhart, G. J., Mohr, C., Kostenidou, E., Lanz, V. A., Bougiatioti, A., DeCarlo, P. F., Prevot, A. S. H., Baltensperger, U., Mihalopoulos, N., Donahue, N. M., and Pandis, S. N.: Aged organic aerosol in the Eastern Mediterranean: the Finokalia Aerosol Measurement Experiment — 2008, Atmos. Chem. Phys., 10, 4167-4186, doi:10.5194/acp-10-4167-2010, 2010.

Jimenez, J. L., Canagaratna, M. R., Donahue, N. M., Prevot, A. S., Zhang, Q., Kroll, J. H., DeCarlo, P. F., Allan, J. D., Coe, H., Ng, N. L., Aiken, A. C., Docherty, K. S., Ulbrich, I. M., Grieshop, A. P., Robinson, A. L., Duplissy, J., Smith, J. D., Wilson, K. R., Lanz, V. A., Hueglin, C., Sun, Y. L., Tian, J., Laaksonen, A., Raatikainen, T., Rautiainen, J., Vaattovaara, P., Ehn, M., Kulmala, M., Tomlinson, J. M., Collins, D. R., Cubison, M. J., Dunlea, E. J., Huffman, J. A., Onasch, T. B., Alfarra, M. R., Williams, P. I., Bower, K., Kondo, Y., Schneider, J., Drewnick, F., Borrmann, S., Weimer, S., Demerjian, K., Salcedo, D., Cottrell, L., Griffin, R., Takami, A., Miyoshi, T., Hatakeyama, S., Shimono, A., Sun, J. Y., Zhang, Y. M., Dzepina, K., Kimmel, J. R., Sueper. D., Jayne, J. T., Herndon, S. C., Trimborn, A. M., Williams, L. R., Wood, E. C., Middlebrook, A. M., Kolb, C. E., Baltensperger U., and Worsnop, D. R.: Evolution of organic aerosols in the atmosphere, Science, 326, 1525–1529, doi:10.1126/science.1180353, 2009.

Johnson, B. T., Shine, K. P., Forster, P. M.: The semi-direct aerosol effect: the impact of absorbing aerosols on marine stratocumulus, Q. J. Roy. Meteor. Soc., 130, 1407–1422, doi:10.1126/science.1180353, 2004.

Kanakidou, M., Seinfeld, J. H., Pandis, S. N., Barnes, I., Dentener, F. J., Facchini, M. C., VanDingenen, R., Ervens, B., Nenes, A., Nielsen, C. J., Swietlicki, E., Putaud, J. P., Balkanski, Y., Fuzzi, S., Horth, J., Moortgat, G. K., Winterhalter, R., Myhre, C. E. L., Tsigaridis, K., Vignati, E., Stephanou, E. G., and Wilson, J.: Organic aerosol and global climate modelling: a review, Atmos. Chem. Phys., 5, 1053–1123, doi:10.5194/acp-5-1053-2005, 2005.

ACPD
12, 21815–21865, 2012

Karl, M., Tsigaridis, K., Vignati, E., and Dentener, F.: Formation of secondary organic aerosol from isoprene oxidation over Europe, Atmos. Chem. Phys., 9, 7003–7030, doi:10.5194/acp-9-7003-2009, 2009.

Karydis, V. A., Tsimpidi, A. P., Fountoukis, C., Nenes, A., Zavala, M., Lei, W. F., Molina, L. T., and Pandis, S. N.: Simulating the fine and coarse inorganic particulate matter concentrations in a polluted megacity, Atmos. Environ., 44, 608–620, doi:10.1016/j.atmosenv.2009.11.023,25 2010.

Knote, C., Brunner, D., Vogel, H., Allan, J., Asmi, A., Äijälä, M., Carbone, S., vanderGon, H. D., Jimenez, J. L., Kiendler-Scharr, A., Mohr, C., Poulain, L., Prévôt, A. S. H., Swietlicki, E., and Vogel, B.: Towards an online-coupled chemistry-climate model: evaluation of trace gases and aerosols in COSMO-ART, Geosci. Model Dev., 4, 1077–1102, doi:10.5194/gmd-4-1077-2011, 2011.

Kuenen, J., Denier van der Gon, H., Visschedijk, A., van der Brugh, H., and Gijlswijk R.: MACC European emission inventory for the years 2003–2007, TNO-report TNO-060-UT-2011-00588, TNO: Netherlands Organisation for Applied Scientific Research TNO, Utrecht, The Netherlands, 2011.

Kulmala, M., Asmi, A., Lappalainen, H. K., Baltensperger, U., Brenguier, J.-L., Facchini, M. C., Hansson, H.-C., Hov, Ø., O'Dowd, C. D., Pöschl, U., Wiedensohler, A., Boers, R., Boucher, O., de Leeuw, G., Denier van der Gon, H. A. C., Feichter, J., Krejci, R., Laj, P., Lihavainen, H., Lohmann, U., McFiggans, G., Mentel, T., Pilinis, C., Riipinen, I., Schulz, M., Stohl, A., Swietlicki, E., Vignati, E., Alves, C., Amann, M., Ammann, M., Arabas, S., Artaxo, P., Baars, H., Beddows, D. C. S., Bergström, R., Beukes, J. P., Bilde, M., Burkhart, J. F., Canonaco, F., Clegg, S. L., Coe, H., Crumeyrolle, S., D'Anna, B., Decesari, S., Gilardoni, S., Fischer, M., Fjaeraa, A. M., Fountoukis, C., George, C., Gomes, L., Halloran, P., Hamburger, T., Harrison, R. M., Herrmann, H., Hoffmann, T., Hoose, C., Hu, M., Hyvärinen, A., Hõrrak, U., Iinuma, Y., Iversen, T., Josipovic, M., Kanakidou, M., Kiendler-Scharr, A., Kirkevåg, A., Kiss, G., Klimont, Z., Kolmonen, P., Komppula, M., Kristjánsson, J.-E., Laakso, L., Laaksonen, A., Labonnote, L., Lanz, V. A., Lehtinen, K. E. J., Rizzo, L. V., Makkonen, R., Manninen, H. E., McMeeking, G., Merikanto, J., Minikin, A., Mirme, S., Morgan, W. T., Nemitz, E., O'Donnell, D., Panwar, T. S., Pawlowska, H., Petzold, A., Pienaar, J. J., Pio, C., Plass-Duelmer, C., Prévôt, A. S. H., Pryor, S., Reddington, C. L., Roberts, G., Rosenfeld, D., Schwarz, J., Seland, Ø., Sellegri, K., Shen, X. J., Shiraiwa, M., Siebert, H., Sierau, B., Simpson, D., Sun, J. Y., Topping, D., Tunved, P., Vaattovaara, P., Vakkari, V.,

ACPD
12, 21815–21865, 2012

Veefkind, J. P., Visschedijk, A., Vuollekoski, H., Vuolo, R., Wehner, B., Wildt, J., Woodward, S., Worsnop, D. R., van Zadelhoff, G.-J., Zardini, A. A., Zhang, K., van Zyl, P. G., Kerminen, V.-M., S Carslaw, K., and Pandis, S. N.: General overview: European Integrated project on Aerosol Cloud Climate and Air Quality interactions (EUCAARI) – integrating aerosol research from nano to global scales, Atmos. Chem. Phys., 11, 13061–13143, doi:10.5194/acp-11-13061-2011, 2011.

Lane, T. E., Donahue, N. M., and Pandis, S. N.: Simulating secondary organic aerosol formation using the volatility basis-set approach in a chemical transport model, Atmos. Environ., 42, 7439–7451, doi:10.1016/j.atmosenv.2008.06.026, 2008.

Liao, H., Henze, D. K., Seinfeld, J. H., Wu, S. L., and Mickley, L. J.: Biogenic secondary organic aerosol over the United States: comparison of climatological simulations with observations, J. Geophys. Res.-Atmos., 112, D06201, doi:10.1029/2006JD007813, 2007.

Majewski, D., Liermann, D., Prohl, P., Ritter, B., Buchhold, M., Hanisch, T., Paul, G., Wergen, W., and Baumgardner, J.: The operational global icosahedral–hexagonal gridpoint model GME: description and high-resolution tests, Mon. Weather Rev., 130, 319–338, doi:10.1175/1520-0493(2002)130<0319:TOGIHG>2.0.CO;2, 2002.

Ming, Y., Ramaswamy, V., Ginoux, P. A., and Horowitz, L. H.: Direct radiative forcing of anthropogenic organic aerosol, J. Geophys. Res., 110, D20208, doi:10.1029/2004JD005573, 2005.

Morgan, W. T., Allan, J. D., Bower, K. N., Esselborn, M., Harris, B., Henzing, J. S., Highwood, E. J., Kiendler-Scharr, A., McMeeking, G. R., Mensah, A. A., Northway, M. J., Osborne, S., Williams, P. I., Krejci, R., and Coe, H.: Enhancement of the aerosol direct radiative effect by semi-volatile aerosol components: airborne measurements in North-Western Europe, Atmos. Chem. Phys., 10, 8151–8171, doi:10.5194/acp-10-8151-2010, 2010a.

Morgan, W. T., Allan, J. D., Bower, K. N., Highwood, E. J., Liu, D., McMeeking, G. R., Northway, M. J., Williams, P. I., Krejci, R., and Coe, H.: Airborne measurements of the spatial distribution of aerosol chemical composition across Europe and evolution of the organic fraction, Atmos. Chem. Phys., 10, 4065–4083, doi:10.5194/acp-10-4065-2010, 2010b.

Murphy, B. N. and Pandis, S. N.: Simulating the formation of semivolatile primary and secondary organic aerosol in a regional chemical transport model, Environ. Sci. Technol., 43, 4722–4728, 2009.

ACPD
12, 21815–21865, 2012

Murphy, B. N. and Pandis, S. N.: Exploring summertime organic aerosol formation in the Eastern United States using a regionalscale budget approach and ambient measurements, J. Geophys.Res., 115, D24216, doi:10.1029/2010JD014418, 2010.

Murphy, B. N., Donahue, N. M., Fountoukis, C., and Pandis, S. N.: Simulating the oxygen content of ambient organic aerosol with the 2-D volatility basis set, Atmos. Chem. Phys., 11, 7859–7873, doi:10.5194/acp-11-7859-2011, 2011.

Myhre, G., Berglen, T. F., Johnsrud, M., Hoyle, C. R., Berntsen, T. K., Christopher, S. A., Fahey, D. W., Isaksen, I. S. A., Jones, T. A., Kahn, R. A., Loeb, N., Quinn, P., Remer, L., Schwarz, J. P., and Yttri, K. E.: Modelled radiative forcing of the direct aerosol effect with multi-observation evaluation, Atmos. Chem. Phys., 9, 1365–1392, doi:10.5194/acp-9-1365-2009, 2009.

O'Donnell, D., Tsigaridis, K., and Feichter, J.: Estimating the direct and indirect effects of secondary organic aerosols using ECHAM5-HAM, Atmos. Chem. Phys., 11, 8635–8659, doi:10.5194/acp-11-8635-2011, 2011.

Penner, J. E., Zhang, S. Y., and Chuang, C. C.: Soot and smoke aerosol may not warm climate, J. Geophys. Res., 108, 4657, doi:10.1029/2003JD003409, 2003.

Pierce, J. R., Leaitch, W. R., Liggio, J., Westervelt, D. M., Wainwright, C. D., Abbatt, J. P. D., Ahlm, L., Al-Basheer, W., Cziczo, D. J., Hayden, K. L., Lee, A. K. Y., Li, S.-M., Russell, L. M., Sjostedt, S. J., Strawbridge, K. B., Travis, M., Vlasenko, A., Wentzell, J. J. B., Wiebe, H. A., Wong, J. P. S., and Macdonald, A. M.: Nucleation and condensational growth to CCN sizes during a sustained pristine biogenic SOA event in a forested mountain valley, Atmos. Chem. Phys., 12, 3147–3163, doi:10.5194/acp-12-3147-2012, 2012.

Pikridas, M., Bougiatioti, A., Hildebrandt, L., Engelhart, G. J., Kostenidou, E., Mohr, C., Prévôt, A. S. H., Kouvarakis, G., Zarmpas, P., Burkhart, J. F., Lee, B.-H., Psichoudaki, M., Mihalopoulos, N., Pilinis, C., Stohl, A., Baltensperger, U., Kulmala, M., and Pandis, S. N.: The Finokalia Aerosol Measurement Experiment – 2008 (FAME-08): an overview, Atmos. Chem. Phys., 10, 6793–6806, doi:10.5194/acp-10-6793-2010, 2010.

Riemer, N., Vogel, H., Vogel, B., and Fiedler, F.: Modeling aerosols on the mesoscale-γ: treatment of soot aerosol and its radiative effects, J. Geophys. Res., 108, 4601, doi:10.1029/2003JD003448, 2003.

Ritter, B. and Geleyn, J.-F.: A comprehensive scheme for numerical weather prediction models with potential applications in climate simulations, Mon. Weather Rev., 120, 303–325, 1992.

ACPD

12, 21815–21865, 2012

Robinson, A. L., Donahue, N. M., Shrivastava, M. K., Weitkamp, E. A., Sage, A. M., Grieshop, A. P., Lane, T. E., Pierce, J. R., and Pandis, S. N.: Rethinking organic aerosols: semivolatile emissions and photochemical aging, Science, 315, 1259–1262, doi:10.1126/science.1133061, 2007.

Robinson, N. H., Hamilton, J. F., Allan, J. D., Langford, B., Oram, D. E., Chen, Q., Docherty, K., Farmer, D. K., Jimenez, J. L., Ward, M. W., Hewitt, C. N., Barley, M. H., Jenkin, M. E., Rickard, A. R., Martin, S. T., McFiggans, G., and Coe, H.: Evidence for a significant proportion of Secondary Organic Aerosol from isoprene above a maritime tropical forest, Atmos. Chem. Phys., 11, 1039–1050, doi:10.5194/acp-11-1039-2011, 2011.

Schell, B., Ackermann, I. J., Binkowski, F. S., and Ebel, A.: Modeling the formation of secondary organic aerosol within a comprehensive air quality model system, J. Geophys. Res., 106, 28275–28293, 2001.

Schnaiter, M., Linke, C., Möhler, O., Naumann, K.-H., Saathoff, H., Wagner, R., Schurath, U., and Wehner, B.: Absorption amplification of black carbon internally mixed with secondary organic aerosol, J. Geophys. Res., 110, D19204, doi:10.1029/2005JD006046, 2005.

Shindell, D. and Faluvegi, G.: Climate response to regional radiative forcing during the twentieth century, Nat. Geosci., 2, 294–300, doi:10.1038/ngeo473, 2009.

Shrivastava, M. K., Lane, T. E., Donahue, N. M., Pandis, S. N., and Robinson, A. L.: Effects of gas particle partitioning and aging of primary emissions on urban and regional organic aerosol concentrations, J. Geophys. Res., 113, D18301, doi:10.1029/2007JD009735, 2008.

Shrivastava, M., Fast, J., Easter, R., Gustafson Jr., W. I., Zaveri, R. A., Jimenez, J. L., Saide, P., and Hodzic, A.: Modeling organic aerosols in a megacity: comparison of simple and complex representations of the volatility basis set approach, Atmos. Chem. Phys., 11, 6639–6662, doi:10.5194/acp-11-6639-2011, 2011.

Simpson, D., Yttri, K. E., Klimont, Z., Kupiainen, K., Caseiro, A., Gelencsér, A., Pio, C., Puxbaum, H., and Legrand, M.: Modeling carbonaceous aerosol over Europe: Analysis of the CARBOSOL and EMEP EC/OC campaigns, J. Geophys. Res., 112, D23S14, doi:10.1029/2006JD008158, 2007.

Spindler, G., Brüggemann, E., Gnauk, T., Grüner, A., Müller, K., and Herrmann, H.: A four-year size-segregated characterization study of particles PM_{10}, $PM_{2.5}$ and PM_1 depending on air mass origin at Melpitz, Atmos. Environ., 44, 164–173, doi:10.1016/j.atmosenv.2009.10.015, 2010.

ACPD
12, 21815–21865, 2012

Stanelle, T., Vogel, B., Vogel, H., Bäumer, D., and Kottmeier, C.: Feedback between dust particles and atmospheric processes over West Africa during dust episodes in March 2006 and June 2007, Atmos. Chem. Phys., 10, 10771–10788, doi:10.5194/acp-10-10771-2010, 2010.

Stern, R., Builtjes, P., Schaap, M., Timmermans, R., Vautard, R., Hodzic, A., Memmesheimer, M., Feldmann, H., Renner, E., Wolke, R., and Kerschbaumer, A.: A model inter-comparison study focussing on episodes with elevated PM_{10} concentrations, Atmos. Environ., 42, 4567–4588, doi:10.1016/j.atmosenv.2008.01.068, 2008.

Stockwell, W. R., Middleton, P., and Chang, J. S.: The second generation regional acid deposition model chemical mechanism for regional air quality modelling, J. Geophys. Res., 95, 16343–16367, 1990.

Tsigaridis, K., Lathière, J., Kanakidou, M., and Hauglustaine, D. A.: Naturally driven variability in the global secondary organic aerosol over a decade, Atmos. Chem. Phys., 5, 1891–1904, doi:10.5194/acp-5-1891-2005, 2005.

Tsimpidi, A. P., Karydis, V. A., Zavala, M., Lei, W., Molina, L., Ulbrich, I. M., Jimenez, J. L., and Pandis, S. N.: Evaluation of the volatility basis-set approach for the simulation of organic aerosol formation in the Mexico City metropolitan area, Atmos. Chem. Phys., 10, 525–546, doi:10.5194/acp-10-525-2010, 2010.

Tsimpidi, A. P., Karydis, V. A., Zavala, M., Lei, W., Bei, N., Molina, L., and Pandis, S. N.: Sources and production of organic aerosol in Mexico City: insights from the combination of a chemical transport model (PMCAMx-2008) and measurements during MILAGRO, Atmos. Chem. Phys., 11, 5153–5168, doi:10.5194/acp-11-5153-2011, 2011.

van der Gon, H. D., Visschedijk, A., van der Brugh, H., and Droge, R.: A high resolution European emission data base for the year 2005, a contribution to UBA–Projekt PAREST: particle reduction strategies, TNO-report TNO-034-UT-2010-01895 RPTML, 2010.

Vogel, B., Fiedler, F., and Vogel, H.: Influence of topography and biogenic volatile organic compounds emission in the state of Baden-Wurttemberg on ozone concentrations during episodes of high air temperatures, J. Geophys. Res., 100, 22907–22928, 1995.

Vogel, B., Hoose, C., Vogel, H. and Kottmeier, C.: A model of dust transport applied to the Dead Sea Area, Meteorol. Z., 15, 611–624, doi:10.1127/0941-2948/2006/0168, 2006.

Vogel, B., Vogel, H., Bäumer, D., Bangert, M., Lundgren, K., Rinke, R., and Stanelle, T.: The comprehensive model system COSMO-ART – Radiative impact of aerosol on the state of the atmosphere on the regional scale, Atmos. Chem. Phys., 9, 8661–8680, doi:10.5194/acp-9-8661-2009, 2009.

ACPD
12, 21815–21865, 2012

Volkamer, R., Jimenez, J. L., Martini, F. S., Dzepina, K., Zhang, Q., Salcedo, D., Molina, L. T., Worsnop, D. R., and Molina, M. J.: Secondary organic aerosol formation from anthropogenic air pollution: rapid and higher than expected, Geophys. Res. Lett., 33, L17811, doi:10.1029/2006GL026899, 2006.

Zanis, P., Ntogras, C., Zakey, A., Pytharoulis, I., and Karacostas, T.: Regional climate feedback of anthropogenic aerosols over Europe using RegCM3, Clim. Res., 52, 267–278, doi:10.3354/cr01070, 2012.

Zhang, Q., Jimenez, J. L., Canagaratna, M. R., Allan, J. D., Coe, H., Ulbrich, I., Alfarra, M. R., Takami, A., Middlebrook, A. M., Sun, Y. L., Dzepina, K., Dunlea, E., Docherty, K., DeCarlo, P. F., Salcedo, D., Onasch, T., Jayne, J. T., Miyoshi, T., Shimono, A., Hatakeyama, S., Takegawa, N., Kondo, Y., Schneider, J., Drewnick, F., Borrmann, S., Weimer, S., Demerjian, K., Williams, P., Bower, K., Bahreini, R., Cottrell, L., Griffin, R. J., Rautiainen, J., Sun, J. Y., Zhang, Y. M., and Worsnop, D. R.: Ubiquity and dominance of oxygenated species in organic aerosols in anthropogenically-influenced Northern Hemisphere midlatitudes, Geophys. Res. Lett., 34, L13801, doi:10.1029/2007GL029979, 2007.

Zhao, C., Liu, X., and Leung, L. R.: The impact of Great Basin Desert dust on the summer monsoon system over southwestern North America, Atmos. Chem. Phys. Discuss., 11, 31735–31767, doi:10.5194/acpd-11-31735-2011, 2011.

ACPD

12, 21815–21865, 2012

Table 1. Oxidation Reactions of the SOA precursors towards the 4 lumped condensable species treated by the VBS version incorporated in COSMO-ART. The non highlighted species and reactions are not treated, when COSMO-ART is coupled with SORGAM.

	SOA Precursors	Description	Oxidation reactions
Anthropogenic	HC_8	Higher Alkanes	$HC_8 + HO \rightarrow HC_8P + 0.75\ XO_2 + H_2O$
	OLT	Terminal Alkenes	$OLT + HO \rightarrow OLTP$
			$OLT + O_3 \rightarrow 0.53\ HCHO + 0.50\ ALD + 0.33\ CO + 0.20\ ORA1 + 0.20\ ORA2 + 0.23\ HO_2 + 0.22\ MO_2 + 0.10\ HO + 0.06\ CH_4$
			$OLT + NO_3 \rightarrow OLN$
			$OLI + HO \rightarrow OLIP$
	OLI	Internal Alkenes	$OLI + O_3 \rightarrow 0.18\ HCHO + 0.72\ ALD + 0.10\ KET + 0.23\ CO + 0.06\ ORA1 + 0.29\ ORA2 + 0.09\ CH_4 + 0.26\ HO_2 + 0.14\ HO + 0.31\ MO_2$
			$OLI + NO_3 \rightarrow OLN$
	TOL	Toluene	$TOL + HO \rightarrow 0.75\ TOLP + 0.25\ CSL + 0.25\ HO_2$
	XYL	Xylene	$XYL + HO \rightarrow 0.83\ XYLP + 0.17\ CSL + 0.17\ HO_2$
	CSL	Cresol	$CSL + HO \rightarrow 0.1\ HO_2 + 0.9\ XO_2 + 0.9\ TCO3 - 0.9\ HO$
			$CSL + NO_3 \rightarrow HNO_3 + XNO_2 + 0.5\ CSL$
Biogenic	ISO	Isoprene	$ISO + HO \rightarrow ISOP$
			$ISO + O_3 \rightarrow 0.58\ HCHO + 0.10\ ACO_3 + 0.14\ CO + 0.28\ ORA1 + 0.25\ HO_2 + 0.08\ MO_2 + 0.25\ HO + 0.09\ H_2O_2 + 0.65\ MACR + 0.1\ MACP$
	API	a-Pinene	$API + OH \rightarrow APIP$
			$API + O_3 \rightarrow 0.65\ ALD + 0.53\ KET + 0.14\ CO + 0.20\ ETHP + 0.42\ KETP + 0.85\ HO + 0.10\ HO_2 + 0.02\ H_2O_2$
			$API + NO_3 \rightarrow OLN$
	LIM	Limonene	$LIM + OH \rightarrow LIMP$
			$LIM + O_3 \rightarrow 0.04\ HCHO + 0.46\ OLT + 0.14\ CO + 0.16\ ETHP + 0.42\ KETP + 0.85\ OH + 0.10\ HO_2 + 0.02\ H_2O_2 + 0.79\ MACR + 0.01\ ORA1 + 0.07\ ORA2$
			$LIM + NO_3 \rightarrow OLN$

ACPD
12, 21815–21865, 2012

Table 2. SOA yields ($\mu g\,m^{-3}$ / $\mu g\,m^{-3}$) using a four-product VBS with the saturation concentrations of 1, 10, 100, 1000 $\mu g\,m^{-3}$ at 298 K. Aerosol density is assumed to be 1.4 $g\,cm^{-3}$.

SOA Precursors	Saturation Concentration ($\mu g\,m^{-3}$) of SOA species			
	1	10	100	1000
HC_8	–	0.3	–	–
OLT	0.0045	0.009	0.06	0.225
OLI	0.0225	0.0435	0.129	0.375
TOL	0.01065	0.2571	0.75	0.96435
XYL	0.075	0.3	0.375	0.525
CSL	–	–	–	–
ISO	0.009	0.03	0.015	0
API	0.10725	0.0918	0.3585	0.6075

ACPD
12, 21815–21865, 2012

Table 3. Description of modeling scenarios performed by COSMO-ART application over Europe during May 2008. All scenarios except for no 1 and 3 are performed using the VBS approach.

Scenario	Simulation dates (May 2008)	Scenario's Description	Objective	Analysis Section
Base-case	1 to 31	VBS approach[1]	OA performance over Europe	4.2
1	1 to 31	SOA chemistry is switched off	Direct radiative effects of SOA	4.3
2	1 to 31	zero SOA boundary conditions[1]	Impact of SOA boundary conditions boundary conditions on OA predictions	4.4.1
3	1 to 10	SORGAM module	SOA chemical module inter-comparison	4.4.2
4	1 to 31	VBS approach[2]	Sensitivity of SOA formation on constant parameters	4.4.3
5	16 to 20	High-NO_x regime[2]	Sensitivity of SOA formation on constant parameters	4.4.3
6	1 to 10	SOA aging is not a sink for OH[1]	Impact of SOA oxidation on inorganic aerosol chemistry	4.4.4
7	11 to 15	biogenic VOCs oxidation is not a source for SOA[1]	Anthropogenic vs. biogenic SOA sources	4.4.5

[1] Aging constant: $k = 2.5 \times 10^{-12}\,cm^3\,mol^{-1}\,s^{-1}$, Enthalpy of vaporization: $\Delta H_{vap} = 75\,kJ\,mol^{-1}$

[2] Aging constant: $k = 1 \times 10^{-11}\,cm^3\,mol^{-1}\,s^{-1}$, Enthalpy of vaporization: $\Delta H_{vap} = 30\,kJ\,mol^{-1}$

ACPD
12, 21815–21865, 2012

Table 4. Prediction skill metrics of COSMO-ART hourly ground total PM_1 OA concentration predictions against measurements from 4 stations (Cabauw, Finokalia, Mace Head, Melpitz) during the EUCAARI campaign in May 2008.

Site	Mean predicted ($\mu g\,m^{-3}$)	Mean observed ($\mu g\,m^{-3}$)	MFB(%) (Eq. 1)	MFE(%) (Eq. 2)	r[a]	No of values
Cabauw (Netherlands)	3.6	4.2	−12	33	0.66	622
Mace Head (Ireland)	1.3	2.4	−48	51	0.37	336
Finokalia (Greece)	3.1	2.5	14	51	0.36	490
Melpitz (Germany)	4.3	5.1	−30	56	0.1	155
Average			−13	45	0.56	1603

[a] r stands for correlation coefficient. The equation for the correlation coefficient is:

$$r = \frac{\sum\left(c_m - \overline{c_m}\right)\left(c_o - \overline{c_o}\right)}{\sqrt{\sum\left(c_m - \overline{c_m}\right)^2 \sum\left(c_o - \overline{c_o}\right)^2}}.$$

ACPD
12, 21815–21865, 2012

Table 5. Mean monthly differences in: total PM_1 hourly concentrations (ΔPM_1) ($\mu g\,m^{-3}$), Secondary Organic Aerosol concentrations (SOA) ($\mu g\,m^{-3}$), the rest PM_1 hourly concentrations (ΔPM_{1rest}) ($\mu g\,m^{-3}$), aitken mode PM_1 hourly concentrations (ΔPM_{aitken}) ($\mu g\,m^{-3}$), accumulation mode PM_1 hourly concentrations (ΔPM_{acc}) ($\mu g\,m^{-3}$), PM_1 water hourly concentrations (ΔAWC) ($\mu g\,m^{-3}$), aerosol optical depth at 550 µm (ΔAOD), short-wave surface radiation ($\Delta sSWR$) ($W\,m^{-2}$), long-wave surface radiation ($\Delta sLWR$) ($W\,m^{-2}$), total surface radiation (ΔsR) ($W\,m^{-2}$), temperature (at 2 m altitude a.s.l.) (ΔT) (K) and total cloud cover (ΔCC) (%), due to SOA chemistry during May 2008 over Europe. Percentage changes of the monthly average values predicted by the base-case simulation are presented inside parenthesis. The simulations are performed by COSMO-ART and are described in Table 3.

Mean monthly differences (base-case–scenario 1) due to SOA chemistry:			absolute value (% base-case)
		SOA	1.8 (100)
ΔPM_1 ($\mu g\,m^{-3}$)	ΔPM_{1rest}		2 (51)
		ΔPM_{ait}	0.2 (5)
		ΔPM_{acc}	0.0 (1) / 0.2 (5)
		ΔAWC ($\mu g\,m^{-3}$)	0.7 (5)
		ΔAOD (550 nm)	0.05 (13)
		ΔCC (%)	−0.05 (0)
ΔsR ($W\,m^{-2}$)		$\Delta sSWR$	−1.2 (−20*) / −1.4 (−20*)
		$\Delta sLWR$	+0.2 (20*)
		ΔT (2m a.s.l.) (K)	−0.1 (59*)

* this is the ratio of SOA to total aerosol effect on radiation and temperature.

ACPD
12, 21815–21865, 2012

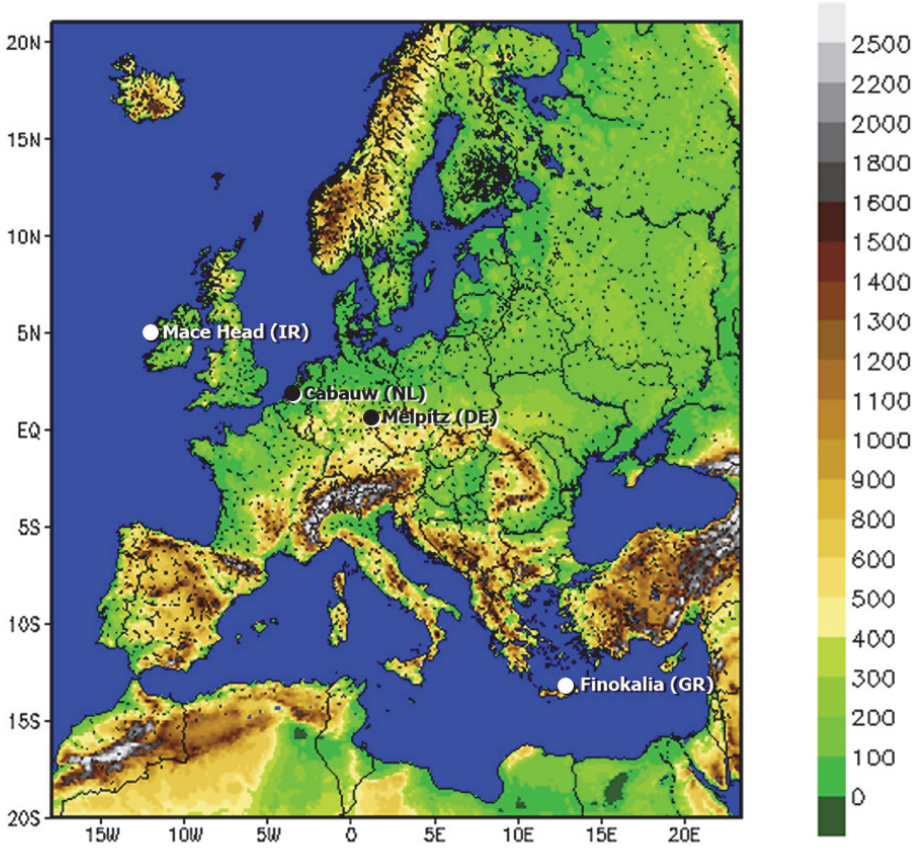

Fig. 1. Application domain and monitoring sites. Outside ticks at 5 degree intervals in rotated geographical co-ordinates. Topography contours at 100 m intervals. (map source: http://www.cosmo-model.org/content/tasks/operational/dwd/default_eu.htm)

ACPD
12, 21815–21865, 2012

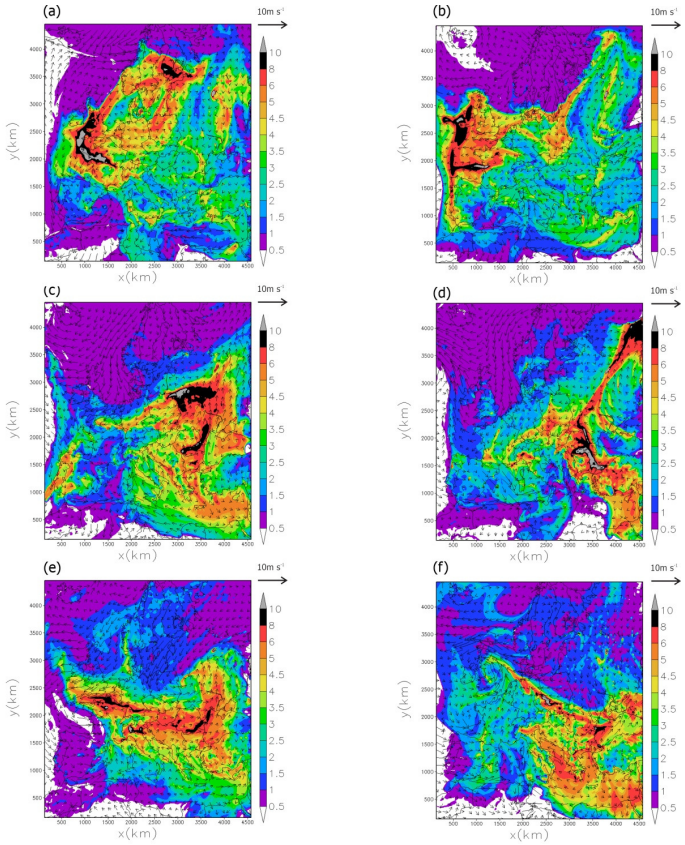

Fig. 2. Spatial distribution of surface Organic Aerosol (OA) concentrations ($\mu g\,m^{-3}$) over Europe, on May 2008, the (date, time in UTC): **(a)** 11, 02:00, **(b)** 12, 11:00, **(c)** 17, 09:00, **(d)** 20, 01:00, **(e)** 24 07:00, and **(f)** 28, 17:00 The arrows indicate surface hourly wind fields. All fields are COSMO-ART predictions.

ACPD
12, 21815–21865, 2012

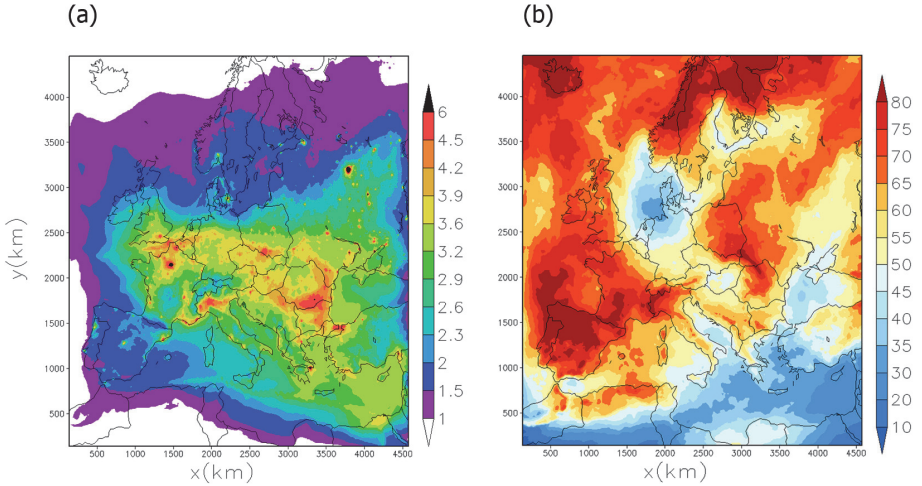

Fig. 3. Spatial distribution of mean monthly: **(a)** Organic Aerosol (OA) concentrations ($\mu g\,m^{-3}$) and **(b)** total cloud cover (%), as predicted by COSMO-ART, during May 2008 over Europe.

ACPD
12, 21815–21865, 2012

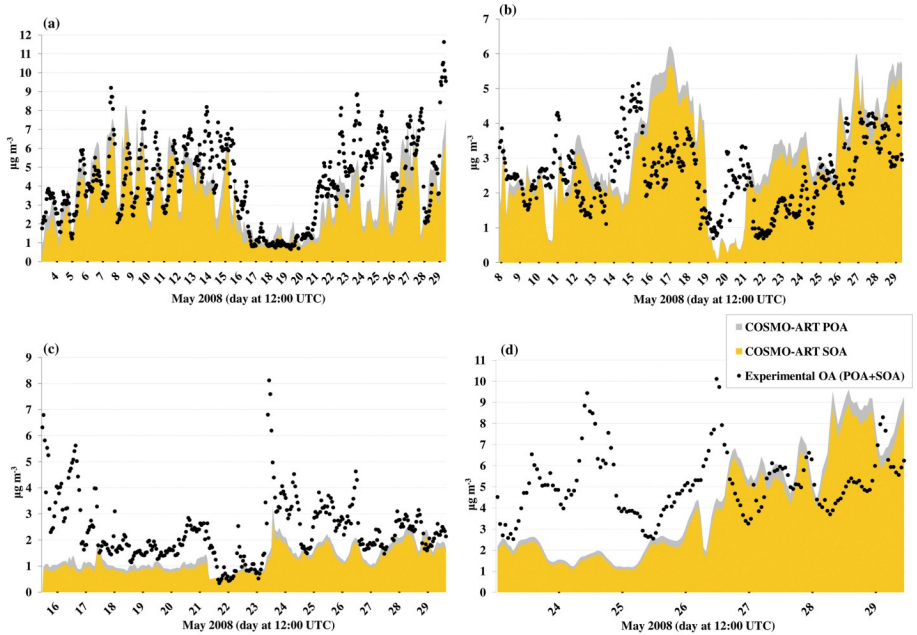

Fig. 4. Comparison of COSMO-ART (total shaded area) and with hourly measurements (black dots) of total PM_1 OA concentrations ($\mu g\,m^{-3}$), during the EUCAARI campaign over: **(a)** Cabauw, **(b)** Finokalia, **(c)** Mace Head and **(d)** Melpitz; the legend applies for all preceding graphs. The contribution of COSMO-ART predicted POA (in grey) and SOA (in yellow) to the total PM_1 OA mass is also shown.

ACPD
12, 21815–21865, 2012

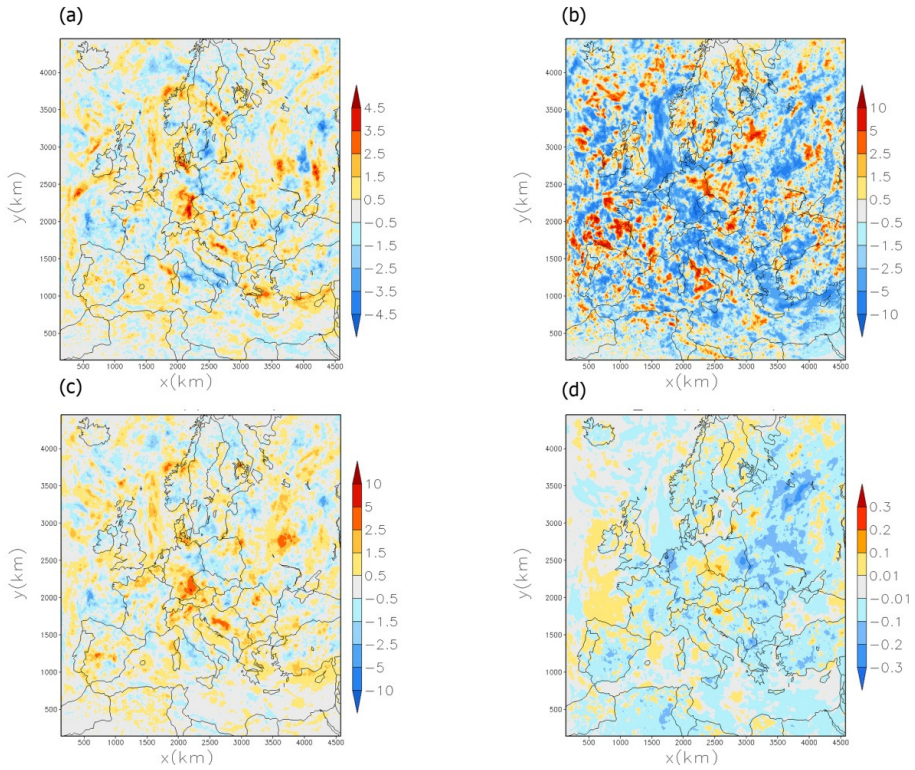

Fig. 5. Spatial distribution of mean monthly differences (base-case simulation–scenario 1) in: **(a)** total cloud cover (%), **(b)** short-wave surface radiation ($W m^{-2}$), **(c)** long-wave surface radiation ($W m^{-2}$), and **(d)** temperature (at 2 m altitude) (K), due to SOA chemistry during May 2008 over Europe. The simulations are performed by COSMO-ART and are described in Table 3.

ACPD
12, 21815–21865, 2012

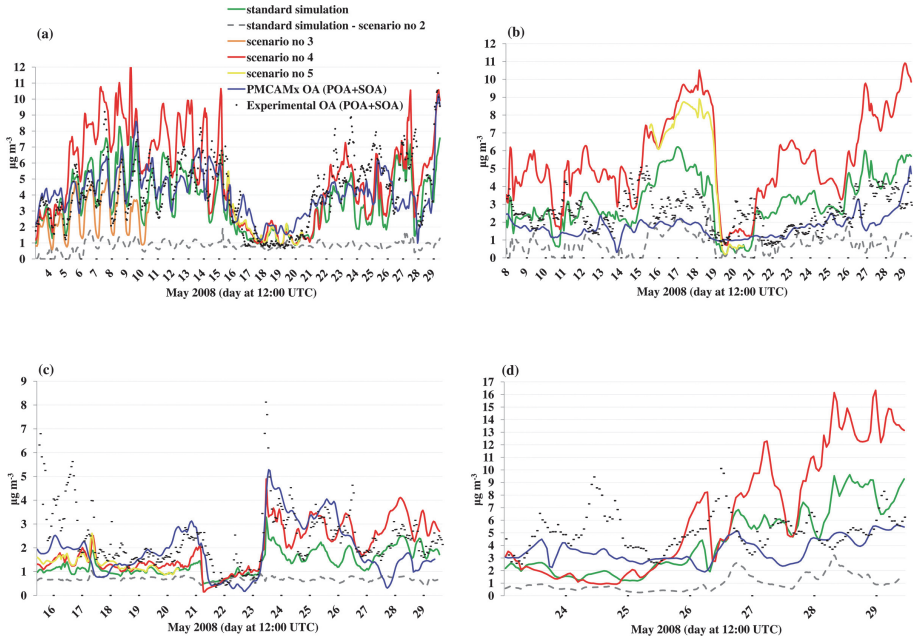

Fig. 6. COSMO-ART results for total PM_1 OA hourly concentrations ($\mu g\,m^{-3}$) from the base-case simulation and scenarios, during May 2008 over: **(a)** Cabauw; the legend applies for all succeeding graphs, **(b)** Finokalia, **(c)** Mace Head and **(d)** Melpitz. Scenarios description is given in Table 3. PMCAMx hourly predictions (blue line) and measurements of total PM_1 OA concentrations ($\mu g\,m^{-3}$) during the EUCAARI campaign (black dots) are also shown.

ACPD
12, 21815–21865, 2012

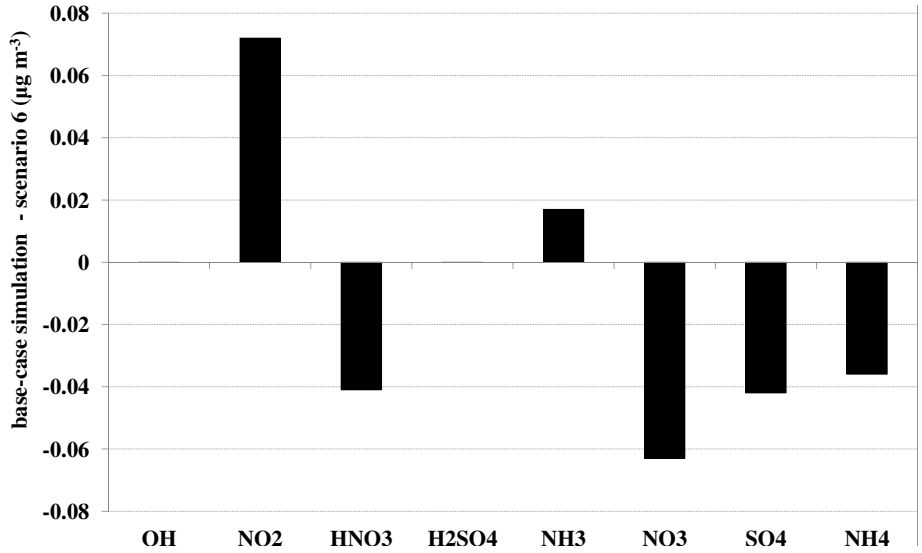

Fig. 7. Mean differences in gaseous and aerosol species ground concentrations ($\mu g m^{-3}$), due to SOA chemical aging over Europe during a 7-day period of May 2008. The simulations are performed by COSMO-ART and are described in Table 3. H_2SO_4 stands for sulfuric acid.

ACPD
12, 21815–21865, 2012

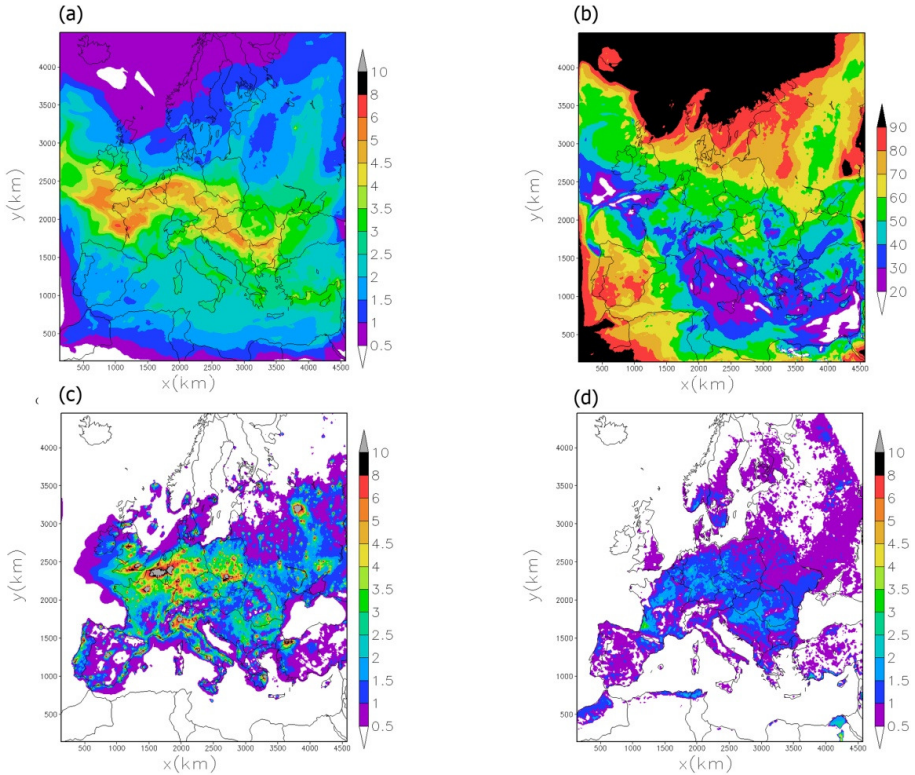

Fig. 8. Spatial distribution over Europe during a 5-day period of May 2008, of surface: **(a)** SOA concentrations ($\mu g\,m^{-3}$) in PM_1 mass, **(b)** biogenic SOA fraction (%), **(c)** anthropogenic SOA gaseous precursor (aromatics, higher alkanes, higher alkenes) concentrations ($\mu g\,m^{-3}$), and **(d)** biogenic SOA gaseous precursor (isoprene and terpenes) concentrations ($\mu g\,m^{-3}$). All values are COSMO-ART predictions.

ACPD
12, 21815–21865, 2012